Journal Name

Perspective

Probing Magnetic Interactions in Metal-Organic Frameworks and Coordination Polymers Microscopically

Received 00th January 20xx,
Accepted 00th January 20xx

DOI: 10.1039/x0xx00000x

www.rsc.org/

Paul J. Saines,*[a] and Nicholas C. Bristowe [a]

Materials with magnetic interactions between their metal centres play both a tremedous role in modern technologies and can exhibit unique physical phenomena. In recent years magnetic metal-organic frameworks and coordination polymers have attracted significant attention because their unique structural flexibility enable them to exhibit multifunctional magnetic properties or unique magnetic states not found in conventional magnetic materials, such as metal oxides. The techniques that enable the magnetic interactions in these materials to be probed at the atomic scale, as long established as key for devloping other magnetic materials, are not well established for studying metal-organic frameworks and coordination polymers. This review focuses on studies where metal-organic frameworks and coordination polymers have been examined by such microscopic probes, with a particular focus on neutron scattering and density-functional theory, the most-well established experimental and computational techniques for understanding magnetic materials in detail. This builds on a brief introduction to these techniques to describe how such probes have been applied to a variety of magnetic materials starting with select historical examples before discussing multifunctional, low dimensional and frustrated magnets. This review highlight the information that can be obtained from such micrscopic studies, including the strengths and limitations of these techniques. The article then concludes with a brief perspective on the future of this area.

Introduction

Materials, which have magnetic interactions between their cations, play a tremendous role in modern technologies including data storage,[1] sensing,[2] actuators[3] and cooling devices[4, 5]. There is also great fundamental interest in the wide variety of unique magnetic states that can emerge, particularly where magnetic interactions are in competition with each other, so called magnetic frustration,[6] or only occur in 1 or 2 dimensions[7]. Conventionally the vast majority of such magnetic materials are alloys or metal oxides, where strong coupling between their magnetic centres facilitate useful properties near room temperatures and there are well-established methods for making the high quality samples required for detailed studies of magnetic materials. It is, however, challenging to modify conventional magnetic materials to incorporate desirable additional properties, such as chirality, ferroelectricity or porosity, required to support the development of more advanced technologies, including spintronics[8]. Similarly it is difficult to realise magnetic oxides and alloys where magnetic chains and sheets are well isolated from each other, as required for low dimensional magnetism and many magnetically frustrated topologies.

In recent years these limitations in conventional magnetic materials has led to tremendous interest in magnetic compounds in which metal cations are linked through organic ligands into an extended structure. The wide diversity of components that can be incorporated in such materials enables them to be readily tailored to incorporate multifunctional properties, as seen in interest in these materials as magnetic sensors for different guest molecules,[9] chiral magnets[10] and multiferroics that combine magnetism with ferroelectric order[11]. The magnetic interactions between cations in these systems can be facilitated through the backbone of the ligand, a functional group such as a carboxylate, or a single coordinating atom; with the strength of magnetic coupling generally increasing for smaller coupling pathways in the absence of conjugation.[12] Depending on their precise topology and extent of porosity such materials are alternatively called metal-organic frameworks (MOFs), coordination networks or coordination polymers. For clarity in this article magnetic materials with covalent bonding connecting cations in two or three dimensions will be described as MOFs to emphasise the focus of this review on those materials with organic ligands; even if they are non-porous as this aspect of the definition of MOFs is still debated[13]. Materials with only 1D extended covalent bonding will be referred to as coordination polymers.

The bulk magnetic properties of MOFs and coordination polymers are readily probed using modern magnetic property characterisation facilities and there are numerous publications that report a wide range of fascinating and potentially useful magnetic properties across this vast class of magnetic materials.[14] The nature of the microscopic interactions that

[a] School of Physical Sciences, University of Kent, Canterbury, CT2 7NH, Kent.

give rise to these properties are then typically inferred based on their crystal structures with very few studies directly probing how the magnetic interactions in MOFs arise from atomic scale correlations. This is in sharp contrast to magnetic oxides and alloys where such direct probing of atomic-scale magnetic interactions using experimental and computational approaches has been well established as crucial in developing the understanding required for their future development.[15, 16] Amongst the techniques for directly probing magnetic interactions neutron scattering and Density-Functional Theory (DFT) are the most widely and prominently used experimental and theoretical techniques. The application of these to magnetic MOFs has tremendous potential to accelerate their development and provide insight into their unique behaviour.

To provide insight into the knowledge that can be gleamed from techniques for probing magnetic interactions in MOFs at the microscopic scale this perspective will set-out a series of case studies that focus on examples of early applications to more recent studies of functional, low dimensional and frustrated magnets, all areas where such materials have gained significant attention. These will highlight how experimental and computational approaches can provide a greater understanding of the origins of magnetic properties at the atomic-scale and of the unique exotic magnetic states that arise in MOFs and coordination polymers. In order to do so, however, we must first provide brief introductions into the two key families of techniques that lie at the heart of the case studies discussed, neutron scattering and DFT, including insight into what has previously restricted their wider application to MOFs and recent advancements that have began to change this outlook.

Neutron Scattering

The detailed understanding of magnetic materials has benefited significantly from rapid advancements in recent years in the use of X-ray based techniques[17] while both muon spin and Mossbauer spectroscopy remain invaluable tools for enhancing the understanding of specific magnetic materials.[18] The dominant experimental techniques for probing magnetic interactions at a microscopic scale in both purely inorganic materials and MOFs still continue to be based on neutron scattering.[15, 16] As established by the pioneering work of Clifford Shull in the 1950s[19] the magnetic spin of the neutron enables it to interact directly with the unpaired electrons in a magnet leading to magnetic neutron diffraction.[15, 16] This can provide information on the alignment of the spin on magnetic atoms compared to the spins of surrounding magnetic atoms in the same way diffraction studies can be used to determine conventional crystallographic structures. Inelastic neutron scattering also occurs, which enables the energy of the magnetic excitations in a material to be probed by measuring the energy lost by neutrons during such events.[15] This gives an indication of the nature of the magnetic dynamics in a system.

The use of neutron scattering to experimentally probe MOFs and coordination polymers has remained restricted because of difficulties stemming from the historical necessity to prepare large multi-gram powder samples or obtain large (> 10 mm^3) sized single crystals, in which the organic ligands are perdeuterated.[16] This arises from the weak interactions of neutrons with samples, which traditionally required large sample volumes and the elimination of the incoherent scattering of hydrogen to obtain data with acceptable signal-to-noise. This poses problems for MOFs because the typical approaches used to make them often make sample scale-up and deuteration time-consuming, expensive and challenging, if not impossible. Worse carefully deuterated but labile protons, such as those on amines or alcohols, can exchange with hydrogen atoms from water in the atmosphere rapidly losing the benefits of this careful treatment.

As foreshadowed by Day, in his introductory review into the use of neutron scattering on molecular-based magnetic materials,[20] modern advances in instrumentation enable neutron diffraction experiments on smaller samples, including powder samples well under a gram in size, opening up new materials to this technique. This is particularly the case at more intense reactor sources such as the Institut Laue-Langevin (ILL), France and the OPAL reactor in Australia and modern spallation sources, namely the ISIS Neutron and Muon Source, Japan Proton Accelerator Research Complex Materials and Life Science Experimental Facility (JPARC MLF) and Spallation Neutron Source (SNS) facilities in the United Kingdom, Japan and North America, respectively. These same advancements in instrumentation have enabled magnetic structures of MOFs to be determined from hydrogenous samples in recent years as the intensities of neutron sources have increased allowing higher sample related backgrounds to be tolerated. This follows from similar results in determining the crystal structures of hydrogenous materials, as set-out by the review of Weller *et al*.[21] Inelastic studies of MOFs still typically require larger sample sizes and deuteration but this may change as the techniques advance further.

Density Functional Theory

The insight gained from experimental studies of magnets at the atomic-scale can be greatly enhanced by computational techniques, most commonly Density-Functional Theory (DFT) based, although the use of this approach to study magnetic phenomena remains challenging particularly for the complex structures adopted by MOFs. Thanks to the seminal Hohenberg and Kohn theorem[22] and the Kohn and Sham ansatz[23], in addition to the numerous advances in computational power and algorithm development, DFT has transformed from a theoretical curiosity to a pivotal technique in many areas of materials research. Indeed, Kohn was awarded the Nobel prize for his contribution, and the DFT community is ever growing, as is the number of undergraduate courses offering dedicated modules on the topic. DFT is a powerful technique able to solve for the electronic ground state of complex materials. It is perhaps the compromise between speed and accuracy that often lends theorists to employ DFT simulations for systems of tens to thousands of atoms. For magnetic materials, the simplest extension of

standard Kohn-Sham DFT is to treat the density of up and down spins separately, without too much computational expense. More generally one can go beyond this so-called collinear-spin approximation, by no longer treating the density as a scalar but a 2x2 matrix that can relax in both direction and magnitude. At this non-collinear spin level,[24] interactions between the lattice and spins are necessarily captured by spin-orbit terms. Whilst often necessary for complex spin orders, non-collinear spin calculations are often taxing and typically become less predictive due to the vast number of potential metastable spin configurations. Similarly, determining not only the spin structure, but simply the ground state atomic structure is problematic in any local minimisation method, where the volume of metastable states is large due to the structural complexity of frameworks and polymers. This becomes even more challenging in framework systems where spin and lattice dynamics become important. The interplay between experiments and DFT is therefore even more crucial than normal in the studies of complex magnetic materials.

Feedback between DFT and experiment is important more generally, since whilst the underlying theory of DFT is in principal exact, several approximations are required for its practical application, which can lead to important limitations. In fact, perhaps the two most well-known limitations are in the study of strongly correlated systems and dispersion effects, both pertinent to magnetic framework materials discussed in this review. Many flavours of dispersion corrections to the local density and gradient generalised approximations (LDA and GGA) to the exchange-correlation energy are now available, and often yield results with a trade-off between accuracy and computational speed (for example, see Grimme[25]). LDA and GGA are also often unsuitable for magnetic materials, yielding qualitatively incorrect ground states, and in these cases more advanced functionals are required to better capture electron correlations. Perhaps the simplest is to artificially add an on-site Coulomb repulsion, U, and inter-site exchange interaction, J, in a Hubbard-like model in what is known as the LDA+U (or GGA+U) approximation.[26] Whilst these two parameters can be self-consistently determined,[27] they often require re-scaling, and so in practice are typically adjusted to match experiment, or, where experiments are not available, fitted to a higher-level theory. Hybrid functionals, which combine LDA or GGA with exact exchange from Hartree-Fock theory, are becoming more widely used in an attempt to overcome the system-dependent parameters of LDA+U, whilst remaining fairly computationally tractable. Going beyond the static mean field theory of DFT, there exist several methods that can better capture electronic correlations, such as dynamical mean field theory (DMFT), quantum chemical or wave function theories, and GW. DMFT is particularly pertinent to frameworks where capturing spin dynamics is important. At this moment in time, these techniques have not commonly been applied to the magnetic frameworks and polymers discussed here, possibly due to limitations of these methods in structurally complex systems, and so we will not discuss them any further in this review. However, we expect these techniques to become increasingly important in years to come, perhaps in combination with DFT, for the predictive modelling of frameworks.

Early Neutron Scattering Studies of Magnetic MOFs

Despite the relative scarcity of studies that probe the magnetic interactions of MOFs microscopically neutron scattering studies of materials that we would now recognise as magnetic MOFs go back at least as far as 1975 where Burlet *et al.*[28] reported the magnetic structures of the $M(Fm)_2{\cdot}2H_2O$ (where M = Mn, Fe, Co and Ni and Fm is formate). These adopt monoclinic structures with two distinct octahedral cation sites. The first of these, the so-called A-site, connect to four identical cations in a plane via formate ligands to form a diamonoid arrangement within the *bc* plane; the A-site cations also have formate links to B-site cations between the layers, with the remaining coordination of the B-sites being completed by bonded to four waters molecules. Magnetic property measurements show these materials are canted antiferromagnets below 4 K for $Mn(Fm)_2{\cdot}2H_2O$ and $Fe(Fm)_2{\cdot}2H_2O$, 5 K for $Co(Fm)_2{\cdot}2H_2O$ and 16 K for $Ni(Fm)_2{\cdot}2H_2O$.[29] Powder neutron diffraction measurements on deuterated samples revealed antiferromagnetic coupling between A-site cations within a plane in all four materials (see Fig. 1). Even at very low temperatures in all cases B-site cations only partially magnetically order with antiferromagnetic coupling to neighbouring A-site cations in three of the four compounds while this is ferromagnetic in $Ni(Fm)_2{\cdot}2H_2O$.[28]

Neutron diffraction revealed that the orientation of the spins varies significantly across the series but can generally be described as either having antiferromagnetic coupling of moments lying in the *ac* plane with ferromagnetic canting towards the *b*-axis or, the reverse, with antiferromagnetic coupled moments lying along the *b*-axis with canting towards the *ac* plane;[28] the precise spin orientations are more complex corresponding to an octahedral axis for Fe and Co cations but not Mn and Ni. In $Mn(Fm)_2{\cdot}2H_2O$ both orientations are observed the latter just below 4 K and the former in a second magnetic phase that arises below 1.7 K, with spin canting towards the *a*-axis, such that there is a net ferromagnetic moment along this direction. In $Fe(Fm)_2{\cdot}2H_2O$ spins align antiferromagnetically in the *ac* plane with a ferromagnetic canting towards the *b*-axis while, in contrast, $Co(Fm)_2{\cdot}2H_2O$ has a spin arrangement with spin components along the *b*-axis antiferromagnetic and ferromagnetic canting towards the *a*-axis. Burlet *et al.*[28] indicated $Ni(Fm)_2{\cdot}2H_2O$ has antiferromagnetic alignment of spins in the *ac*-plane but were unable to resolve the small degree of spin canting in this compound. The inability to resolve spin canting is a common limitation of neutron diffraction studies, particularly where the canting angle is small and in this case it was not until a study by Jorgensen *et al.*[30], some 35 years later, that ferromagnetic canting was found towards the *b*-axis using modern instrumentation.

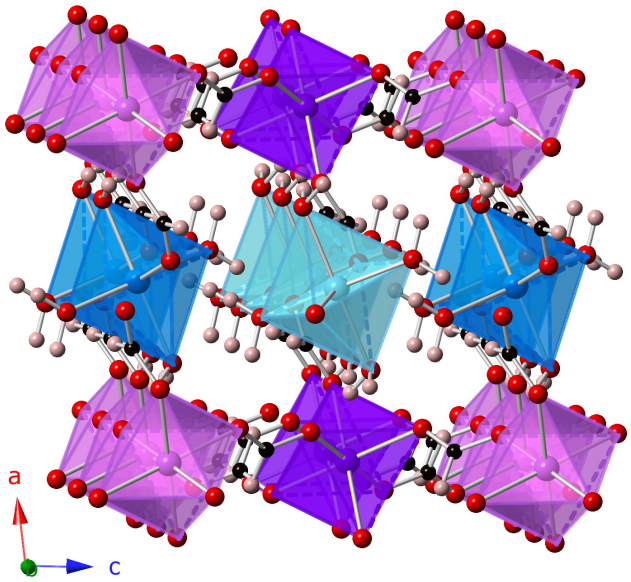

Fig. 1: Crystal structure of the $M(Fm)_2{\cdot}2H_2O$ viewed along the *b*-axis with the A-site cations shown in purple and the B-site cations shown in blue.[28] Antiferromagnetic coupling is shown by polyhedra being light or dark colours for the two respective spin orientations. Carbon, oxygen and hydrogen atoms are black, red and pink.

Precise spin orientations cannot be determined from magnetic property measurements from powders and, while studies of suitable single crystals potentially allow some insight into spin orientation, they lack the precision provided by neutron diffraction. The observed magnetic configurations in the $M(Fm)_2{\cdot}2H_2O$ compounds are considered to reflect a balance between Ising-like single ion anisotropy and dipole-interactions; the former dominates for Fe and Co causing their moments to lie along octahedral axes, with their different electron configuration leading the moment of Fe to preferentially align along the axial direction of the octahedra while the spins of Co prefers to lie in the equatorial plane. For Mn and Ni, where single ion anisotropy is much smaller, dipole-interactions dominate in their ground states and the precise direction in which their moments lie in the *ac* plane has no relationship to an octahedral axes. The spin reorientation of the Mn cations at higher temperatures is considered to be a result of finely balanced interactions, which often lead to complex magnetic behaviour.

The analogous Cu-containing phase is a tetrahydrate, antiferromagnetic $Cu(Fm)_2{\cdot}4H_2O$. This has a significantly different monoclinic structure, due to the Jahn-Teller distortion of the Cu cations, with layers of octahedral Cu cations bridged by formate ligands in the *ab*-plane but capped by water molecules in the axial positions, such that the strongest interlayer interactions are through hydrogen bonding via water molecules between the layers.[31] Burger *et al*.[32] established, using a combination of conventional and polarised single crystal neutron diffraction, that below 17 K, $Cu(Fm)_2{\cdot}4H_2O$ adopts a three dimensionally ordered structure with Cu spins arranged in an antiferromagnetic square lattice with spins lying in the *ac* plane at an angle of 8° from the *a*-axis. Adjacent layers are aligned antiferromagnetically; the coupling between planes is much weaker compared to that within the layers, with a J_{inter}/J_{intra} on the order of 10^{-5} determined from NMR studies,[33] but, perhaps somewhat surprisingly, these residual interactions are still strong enough to support the observed 3D long range order.

Since J_{intra}/k_B in $Cu(Fm)_2{\cdot}4H_2O$ was determined to be 71.5 K from magnetic property measurements there is a large temperature regime where this material acts as a 2D antiferromagnetic square lattice;[34] this is akin to the antiferromagnetic interactions in CuO_2 units in the high T_c cuprate superconductors, leading to renewed interest in $Cu(Fm)_2{\cdot}4H_2O$ in the early 1990's. Fits to spin waves observed in inelastic neutron scattering from a single crystal sample by Clarke *et al*.,[34] one of the first such studies on a MOF, confirmed the material to be a spin ½ 2D Heisenberg antiferromagnet; later fitting to the spin wave energy measured by more extensive inelastic scattering measurements suggested a J_{intra}/k_B of 73(3) K between Cu cations and a very weak Ising anisotropy of less than 0.06 K, confirming Heisenberg behaviour.[35] Inelastic neutron scattering studies by Ronnow *et al*.[36] across a much wider temperature range indicated that there was no-evidence of a cross-over to a Quantum Critical regime, from the correlation lengths and inelastic scattering amplitude, likely a result of interlayer coupling becoming significant before this occurs. As will be highlighted further later in this review this combined approach of using elastic and inelastic neutron scattering to understand low dimensional magnetic phases is particularly powerful to understanding these complex states. Neutron diffraction provides insight into the ground state of these materials, where coupling between low dimensional motifs is strong enough for long-range magnetic order to emerge while neutron spectroscopy provides a direct measurement of the energy scales of the different coupling interactions in a material.

Weakly Ferromagnetic Frameworks

Distinguishing the cause of weak ferromagnetic properties in MOFs as identified from bulk magnetic property measurements can be challenging. The small net ferromagnetic moments in such materials, which are well below that expected for full ferromagnetic alignment of the spins in a compound, can arise from: 1) spin canting, as already discussed in the $M(Fm)_2{\cdot}2H_2O$ phases,[28] which is where spins of antiferromagnetically coupled centres are not precisely antiparallel and commonly results from Dzyaloshinskii-Moriya (DM) interactions, 2) ferrimagnetism where, despite MOFs commonly having only cations in one spin state, a complex pattern of primarily antiferromagnetic interactions can lead to more spins pointing in one direction than in an antiparallel orientation or 3) simply suffer from small-unidentified ferromagnetic impurities. As we will show below the ability of neutron scattering, in particular diffraction, to directly probe the coupling between neighbouring atoms and their spin alignments allows these three possibilities to be distinguished

between, albeit with some limitations for resolving small canting angles.

A good example of such a study where ferromagnetic-like features are observed but whose origin was not clearly assigned from bulk susceptibility measurements is $Mn_3(suc)_2(ina)_2$ (suc – succinate and ina – isonicotinate). This monoclinic compound contains two crystallographically distinct octahedral Mn cations which are arranged in chains aligned along the *b*-axis with two identical Mn2 cations sharing edges and these units connected to each other via corner-sharing with a single Mn1 cation (see Fig. 2).[37] Nearest neighbour chains are bridged through the carboxylate group from succinate ligands and, with greater spacing, along the *c*-axis by the isoniccotinate ligand. Despite only containing d^5 Mn this material was initially diagnosed as a collinear ferrimagnet below 5 K by Zeng *et al*.[37] based on interpretation of the magnetic property measurements, with Mn2 cations in a chain proposed to align ferromagnetically with each other but antiferromagnetically to Mn1. Fabelo *et al*.[38] carried out a combined neutron powder and single crystal diffraction study to test this hypothesis, which were notably both done on a hydrogenous sample with 30 % of atoms being hydrogen in this material. This confirmed the coupling pattern suggested by Zeng et al.[37] but revealed it is not a simple collinear ferrimagnet. While the ordered moment on each site is close to 4 μ_B and their largest spin components, along the *a*-axis, are coupled antiferromagnetically to each other they are far from being collinear with the magnetic moment of Mn1 aligned near the [201] direction while Mn2 is close to the $[\bar{4}\bar{2}1]$ axis.[38]

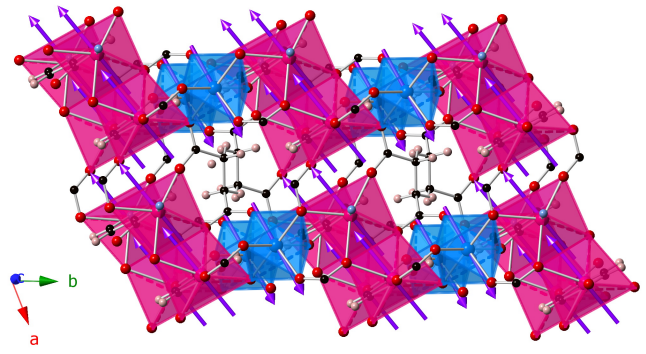

Fig. 2: The structure of $Mn_3(suc)_2(ina)_2$ shown parallel to the layers with Mn1 and Mn2 cations in blue and pink, respectively.[38] The orientation of the magnetic spins are shown by purple arrows and all other colours are as in Fig. 1.

$(DMA)Fe^{3+}Fe^{2+}(Fm)_6$ (DMA is dimethylammonium), which adopts a rhombohedral niccolite-like structure, is another example of a ferrimagnet below 37 K, with N-type behaviour that leads to it exhibiting negative susceptibility at low temperature in modest fields.[39] This material contains octahedral iron connected to six other metal centres of the opposite oxidation state by formate ligands leading to the Fe^{2+} and Fe^{3+} cations occupying alternate layers with disordered dimethylamine filling the pores at room temperature. Negative magnetic susceptibility in N-type ferrimagnets arises from both types of cations ordering at the same temperature but with the ordered moment of the one with the overall lower moment, in this case Fe^{2+}, rising faster initially on cooling than the other, Fe^{3+}.[39] Single crystal magnetic property measurements suggested that the easy axis is along the *c*-axis and exchange bias-like asymmetry was noted in the position of the magnetisation measurements in all cases below the compensation temperature, at which negative magnetic susceptibility occurs, which suggests a highly anisotropic internal magnetic field.[39]

Heat capacity measurements of $(DMA)Fe^{3+}Fe^{2+}(Fm)_6$ show a series of three phase transitions in this material at 155 K, 37 K and 4.8 K.[40] The microscopic nature of these transitions was probed using a combined single crystal and powder neutron diffraction study, again on a hydrogenous sample (38 atom % hydrogen), with a total of only 250 mg used for the powder diffraction experiment. The transition at 155 K was found to be a 3-fold order-disorder transition, missed in the previous X-ray structural characterisation of this material, from $P\bar{3}1c$ *to* $R\bar{3}c$ symmetry associated with the ordering of the dimethylamine cation. Below the magnetic ordering temperature additional scattering was detected that indexed on the crystallographic unit cell, indicating a magnetic structure with a **k**-vector of 0 i.e. that the unit cell of the magnetic structure is the same size as that of the crystallographic structure. Representation analysis was used to calculate all the irreducible representations (irreps) that correspond to the Γ-point of the Brillouin zone, which corresponds to this **k**-vector.[41] In this context irreps are the simplest mathematical representation of ways in which the magnetic order can lower the symmetry of the structure. The basis vectors that obey the symmetry of these irreps, and their linear combinations, are the detailed descriptions of all the possible magnetic structures for a given magnetic cell. Use of these basis vectors enables all possible models of the magnetic structure to be identified and comprehensively tested against the data, avoiding the need for an individual to develop such possibilities in a more arbitrary fashion, which is particularly helpful for complex magnetic MOFs. The magnetic structure determined from this process has Fe^{3+} cations with moments aligned along the *c*-axis and antiferromagnetically coupled to those on the Fe^{2+} sites, which are canted slightly towards the $<1,\bar{1},0>$ axis. The direction in which the component of the magnetic moment of the Fe^{2+} cations points in the *ab* plane points is rotated by a 3_1 screw axis, such that they follow a ABCDEFA packing sequence between different layers; this is a complex deviation from pure ferrimagnetic behaviour that cannot be observed from bulk magnetic property measurements. The ordering of the Fe^{2+} sites appears greater at higher temperatures while the Fe^{3+} sites order to a greater extent at lower ones, confirming the proposed N-type ferrimagnetism. Despite suggestions that the transition at 4.8 K is related to a subtle change in magnetic structure there was no indication of this from the neutron diffraction measurements, although the possibility of subtle spin canting cannot be ruled out, particularly given the high background caused by the significant hydrogen present in the compound.[40]

$(DMA)Fe^{3+}M^{2+}(Fm)_6$ variants with Co^{2+} and Mn^{2+} have also been reported.[42] Magnetic property measurements of

$(DMA)Fe^{3+}Co^{2+}(Fm)_6$ are consistent with a ferrimagnet below 33 K but negative magnetic susceptibility is not observed in this case, suggesting that the ordering of the Co(II) cations occurs at an equal or slower rate compared to Fe(III). $(DMA)Fe^{3+}Mn^{2+}(Fm)_6$, in which both transition metals adopt a d^5 configuration, was suggested to be a spin canted antiferromagnet below 36 K. Neutron powder diffraction did not reveal any ordering of the organic cation in these compounds and the magnetic structures were again indexed on a **k**-vector of 0.[43] In this case it was difficult to precisely measure the magnetic reflections due to the high background from the hydrogenous samples and weak magnetic reflections, which are superimposed on stronger reflections caused by scattering from the crystallographic structure. To compensate for these difficulties potential magnetic structures were deduced from representation analysis. Fits were then carried out against the difference patterns determined by subtracting a pattern collected well above the magnetic ordering temperature, at 45 K, from the 2 K pattern, in which magnetic order is complete, to enable the magnetic scattering to be fitted independently of the crystal structure. As for $(DMA)Fe^{3+}Fe^{2+}(Fm)_6$ the M(II) and Fe(III) sites couple antiferromagnetically but in these hetereometallic frameworks the moments largely lie in the *ab* plane with only a small component along *c*.

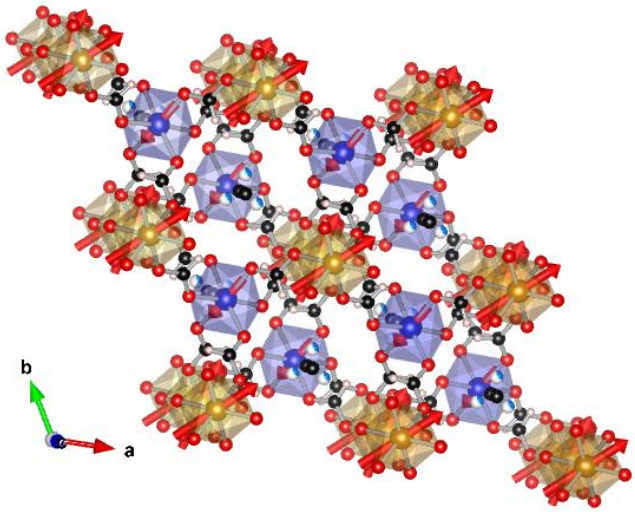

Fig. 3: Structure of $(DMA)FeMn(Fm)_6$ with the Co and Fe cations shown in blue and brown respectively with their spin orientations shown by the red arrows.[43] All other colours are as in Fig. 1.

The magnetic structures of these heterometallic formates adopt *C*2′/*c*′ monoclinic magnetic structures but the diffraction pattern does not show any symmetry lowering from the trigonal crystal structure, preventing the orientation of the magnetic moment in the *ab* plane being directly determined.[43] This is a common problem with solving the magnetic structure of high symmetry phases. DFT calculations based on the GGA+U approximation, however, indicated that in $(DMA)Fe^{3+}Co^{2+}(Fm)_6$ the easy axis of the Co ions is at an angle of 60° from the *a*-axis direction and on the basis of that constraint the magnetic moments of the Co cations were refined to be close to the $[\bar{2},\bar{2},\bar{1}]$ direction while the Fe(III) cation moments are along the [2,3,1] and [3,2,1] vectors alternating between different layers.[43] Fe^{3+} has a higher ordered moment so $(DMA)Fe^{3+}Co^{2+}(Fm)_6$ is another non-collinear ferrimagnet. Using the [2,3,1] alignment of the Fe moments in $(DMA)Fe^{3+}Mn^{2+}(Fm)_6$ as a starting point the magnetic moments of the Mn cations were then found to be along the $[\bar{1},\bar{1},0]$ axis (see Fig. 3). DFT calculations explain the significant difference in the spin orientation between the homometallic and heterometallic compounds in this series as resulting from the easy axis of Fe^{2+} being along the *c*-axis while, as mentioned above, that of Co is close to being along the [1,1,0] direction; these easy axes determine the direction the spins lie in these materials due to the lack of significant single ion anisotropy in d^5 Fe^{3+}. Since in $(DMA)Fe^{3+}Mn^{2+}(Fm)_6$ both cations are close to isotropic the resulting magnetic structure is likely a result of dipolar coupling.

Multiferroic Frameworks

While the niccolite-like $(DMA)Fe^{3+}M^{2+}(Fm)_6$ series has drawn significant attention for both featuring magnetic properties and electronic ordering of the A-site cation the later does not lead to a polar structure.[40] $Cr(Aep)(Cl)(H_2O)$ (Aep is ammoniumethylphosphonate), in contrast is a polar material which has been found to exhibit magnetoelectric coupling.[44, 45] It adopts a lamellar structure with alternating inorganic and organic layers with the chloride and organic molecules oriented along this axis. The inorganic layers have square-pyramidal Cr^{2+} cations with four oxygen atoms in the basal plane from the water and phosphonate ligands, with neighbouring Cr^{2+} along both directions in the layers bridged through the phosphonate. $Cr(Aep)(Cl)(H_2O)]$ orders as a canted antiferromagnet below 6 K, with an estimated canting angle of 4°.[44, 46] An anomaly in the dielectric constant at the magnetic ordering temperature suggested the presence of magnetodielectric coupling.[45] An applied magnetic field was shown to directly influence the dielectric constant both above the magnetic ordering temperature and, an order of magnitude more strongly in the ordered phase; both exhibiting a quadratic dependence.

Neutron diffraction on deuterated $Cr(Aep)(Cl)(H_2O)$ indicated the magnetic **k**-vector of 0 and, using representation analysis, the magnetic structure was determined to feature ferromagnetic coupling within the inorganic planes with antiferromagnetic coupling between these.[46] This structure belongs to the magnetic space group $P2_1$, which allows for a magneotelectric effect and for spin canting, although none of the latter was resolved likely due to the small extent involved. To understand the dominant magnetic interactions in more detail, DFT calculations with the GGA+U exchange correlation functional were employed, with values of U = 3 and 4 eV for Cr.[46] Four nearest neighbour exchange interactions (one interlayer and three intralayer) were determined from total energy calculations of appropriately chosen spin configurations. In agreement with experiment, the interlayer exchange was found to be antiferromagnetic, whilst all three

intralayer exchanges ferromagnetic. The largest of the intralayer exchange interactions was found to be a result of mediation through phosphonate groups linking $[Cr(II)O_4Cl]$ units, consistent with the anticipated dominant super-superexchange interactions. The authors finally performed spin-orbit calculations to determine the easy axis, which was found to lie perpendicular to the layers as observed from the ordering direction in the magnetic structure. Single-ion anisotropy was found to be substantially stronger than the spin exchanges, likely responsible for a direct transition to a weakly ferromagnetic state rather than via an intermediate antiferromagnetic phase.

$AM(Fm)_3$ (where A is a molecular cation and M is Mn, Fe, Co, Ni or Cu) frameworks, which adopt perovskite or chiral hexagonal structures, exhibit polar A-cation order and are therefore of interest as potential multiferroics.[11] While perovskite structures with this stoichiometry, including the archetypical $(DMA)M(Fm)_3$ phases,[47] have drawn the most attention neutron scattering studies of these materials remain scarce[48]. Recently, however, Lawler *et al.*[49] reported a neutron study on both the magnetic and ferroelectric phase transitions in the chiral hexagonal $(NH_4)B(Fm)_3$ (B = Mn, Fe, Co or Ni) series. Previous single crystal X-ray diffraction measurements by Wang *et al.*[50] revealed that these materials adopt a $P6_322$ structure at room temperature wherein BO_6 octahedra are connected to six neighbours via formate ligands. This forms a bidimensional triple helix with ammonium cations sitting disordered in the chiral hexagonal channels along the *c*-axis. Differential scanning calorimetry (DSC) suggested the presence of phase transitions at 254 K, 212 K, 191 K and 199 K for Mn, Fe, Co and Ni.[51] Low temperature single crystal X-ray diffraction studies showed that for Mn, Fe and Co these are associated with a phase transition to a polar $P6_3$ structure in which the NH_4^+ cations order, driven by hydrogen bonding, so that the NH_4^+ cations point up in two-thirds of the channels and down in the other.[51] Dielectric permittivity and polarisation property measurements were consistent with the low temperature state being ferroelectric, with the frequency dependence of the former suggesting relaxor-type properties. Magnetic property characterisation suggested these materials are canted antiferromagnets with ordering temperatures of about 8 K, 9 K, 10 K and 30 K for Mn, Fe, Co and Ni, respectively, with canting angles of less than 0.2° based on remnant magnetization.[50, 51] This Is consistent with these materials being multiferroic.

Using neutron powder diffraction on deuterated samples Lawler *et al.*[49] showed that the disordered NH_4^+ cations in the high temperature phase are best modeled as two distinct molecules whose central N atoms are slightly offset from each other along the channel. This is consistent with rapid fluctuations of these molecules but on a timescale longer than neutron scattering interactions. While neutron diffraction confirmed a transition to the $P6_3$ polar state for Mn, Fe and Co the peaks indicative of this transition were absent in the Ni phase even at 1.5 K. Since in the other compounds in this series decreasing cation size is associated with suppressing this transition to lower temperatures through increasing the chemical pressure on the pore space it appears that the smaller size of the Ni cation is enough to suppress this entirely and that the feature in the DSC may relate to a transition that does not affect the average crystal structure.[49, 51]

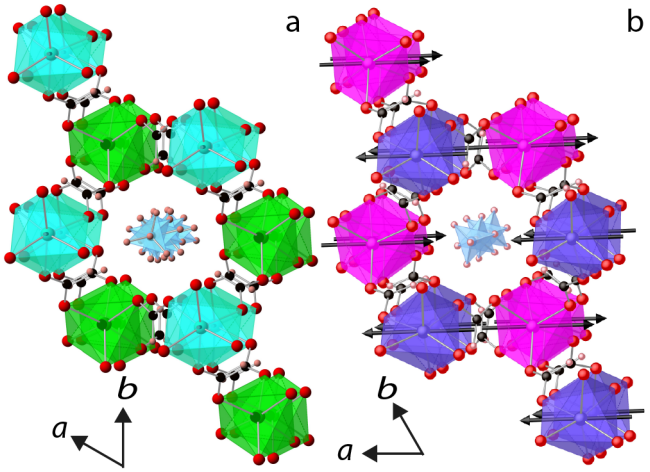

Fig. 4: Magnetic structures of $NH_4Ni(Fm)_3$ (a) and $NH_4Co(Fm)_3$ (b) showing the different spin orientations in these two compounds as black arrows.[49] The spins in $NH_4CO(Fm)_3$ are shown arbitrarily orientated along the *a*-axis and the two different coloured octahedral in each structure correspond to two spin orientations in this antiferromagnetic structure. The NH_4 cations are shown as blue polyhedral and are disordered in (a) and ordered in (b). All other colours are as in Fig. 1.

Additional reflections corresponding to magnetic order were observed below the magnetic ordering temperature with all structures indexed on a **k**-vector of 0.[49] Distortion mode analysis was used to determine possible magnetic structures by identifying the distortion mode irreps, and associated order parameters, compatible with the parent crystallographic symmetry at the appropriate reciprocal-space **k**-point.[52] The order parameters of an irrep, individually or in combination, then define the precise magnetic structure of a material. The difference between this and representation analysis is subtle and depends on whether the basis of the analysis is done with direct regard to space group symmetry or not.[41, 52] The two approaches can yield distinct magnetic structures as well as many in common, although it is the authors' experience that for MOFs and coordination polymers, whose crystallographic symmetry is already low, these differences are far less common than in highly symmetric oxides. In this case two distinct magnetic structures are adopted by members of this family, which differ in their spin direction but retain all nearest-neighbour antiferromagnetic coupling (see Fig. 4). $(NH_4)Mn(Fm)_3$ and $(NH_4)Co(Fm)_3$ adopt magnetic structures in which the spins are all collinear and lie in the *ab*-plane, lowering the magnetic symmetry to monoclinic.[49] As for the heterometalic $(DMA)Fe^{3+}M^{2+}(Fm)_6$ phases the diffraction patterns essentially retain hexagonal symmetry so it is not possible to determine the spin direction in the *ab*-plane.[43] In contrast $(NH_4)Fe(HCO_2)_3$ and $(NH_4)Ni(HCO_2)_3$ have their spins aligned along the *c*-axis.[49] It is not possible to resolve the spin canting directions in any of these materials, as already noted a common limitation of neutron diffraction where canting angles are small. Noticeably none of these materials adopt a chiral

magnetic structure, despite the symmetry of their parent chiral crystal structure. As will become clear in the following section this is far from unusual.

That the magnetic structures of the $(NH_4)B(Fm)_3$ frameworks have a dependency on whether they have an odd number of *d*-electrons, as for Mn and Co, or an even number as for Fe and Ni, is usual and has not been clearly explained.[49] By comparison to the $M(HCO_2)_3{\cdot}2H_2O$ series[28] the difference between Fe and Co could relate to their different electronic configurations leading to different easy axis while the precise balance of small levels of single ion anisotropy, caused by distortions from ideal octahedral geometry, and dipole-dipole coupling in Mn and Ni cause them to adopt different magnetic structures. Arguing against this none of the spin directions in these structures lie along octahedral axes and, while by 1.5 K, Mn and Ni have the expected ordered effective magnetic moment, the ordered moments for Fe and Co are well below that expected for these cations, with their temperature dependence having saturated, which suggests they are not aligned along an easy axis.[49] There are no other clear structural trends that would explain these different magnetic structures so the cause of this requires further investigation. DFT studies of this system are likely to provide a useful insight, however the only report which we are aware of did not perform spin-orbit calculations to investigate the easy axes[53]**.** This study did, however, make the interesting prediction that the Sc and Cr analogues could display ferromagnetic ordering, based on GGA+U calculations with U = 4 and 3.5 eV, respectively; neither of these cations has been incorporated into a published $AB(Fm)_3$ phase with the incorporation of Sc^{2+} particularly unlikely as this oxidation state is rarely observed.

Chiral Magnetism

Materials that combine magnetic order and chirality are of significant interest for their potential to exhibit X-ray magnetochiral dichroism, useful for megahertz and gigahertz optics,[54] and as skyrmions hosts, which have potential for data storage.[55] MOFs have attracted significant interest for such properties because they often adopt chiral structures, either because they incorporate chiral building blocks, or as seen in the $(NH_4)M(Fm)_3$ series,[49] their complex structures allow chiral structures built from non-chiral building blocks. As already highlighted by $(NH_4)M(Fm)_3$, however, having a chiral crystal structure does not necessarily correlate with chiral magnetic symmetry. Another example of this is $[Cr(CN)_6][Mn((S)\text{-}1,2\text{-}diaminopropane)(H_2O)]H_2O$, which despite containing a chiral ligand, was found to adopt $P2_12_12_1$ orthorhombic symmetry and feature a simple collinear antiferromagnetic alignment of alternating Cr and Mn cations.[56]

$Fe(pyrimidine)_2Cl_2$, initially appears a more promising candidate for chiral magnetism adopting a chiral 3D structure, in $I4_122$, despite being built from achiral building blocks.[57] It has FeN_4Cl_2 units connected via pyrimidine ligands and has been shown by bulk susceptibility measurements to exhibit weak ferromagnetism around 6 K with a significant ferromagnetic component of 0.93 μ_B per Fe atom. Powder neutron diffraction on a hydrogenated sample (35 atom % hydrogen) reveals the ordered magnetic structure has a **k**-vector of 0, which can be viewed as ferromagnetic aligned layers of Fe cations but is built from antiferromagnetic superexchange coupling through the pyrimidine ligand.[57] Mössbauer results showed a 59(1)° angle between the magnetic spin direction and the principle electric field axis, indicated by DFT calculations using hybrid functionals to be along the Fe-Cl bonds; using this and the magnitude of the ferromagnetic component observed from magnetic susceptibility measurements, it was determined that the magnetic moments lie close to the *b*-axis with a 14**°** ferromagnetic cant towards the *a*-axis. This magnetic structure is not chiral and the unusually large canting angle is interpreted as arising from a balancing of antiferromagnetic coupling and preference for an easy axis direction, that rotates 90**°** between layers.

$[Ru(bpy)_2(ppy)][MnCr(ox)_3]$ (bpy – 2,2'-bipyridine, ppy – 2-phenylpyridine and ox – oxalate) attracted interest as one of the first 3D optically active molecule-based materials with magnetic order, adopting a $P2_13$ cubic structure.[58] It is based on optically active cationic and anionic units with the same handedness incorporated into a structure with helical chains of [MnCr(ox)], which are also bridged by the oxalate ligand, with the cationic $[Ru(bpy)_2(ppy)]$ sitting in the pore space between chains. Bulk property measurements indicate it has a Curie temperatures of 5.8 K,[58] below which temperature powder neutron diffraction measurements on a 1 g deuterated sample reveal additional intensity on the nuclear reflections, consistent with a structure with a **k**-vector of 0.[59] Fits to the difference between patterns collected below and well above the magnetic ordering temperature give the best fit when all Mn(II) and Cr(III) ions are ferromagnetic, with moments of 4.6(3) μ_B and 2.9(3) μ_B.

It was not possible to distinguish if the moment in $[Ru(bpy)_2(ppy)][MnCr(ox)_3]$ lies along a crystallographic axis or a C_3 body diagonal axis because of the cubic symmetry of the diffraction patterns. Fabrice *et al*.[59] asserted that the magnetic space group of $[Ru(bpy)_2(ppy)][MnCr(ox)_3]$ is likely to be $P2_12'_12'_1$ on the basis that an Fe^{3+} analogue has its magnetic moments aligned along the [100] direction, as determined by Mössbauer spectroscopy. While this assertion is far from certain due to their different electronic configurations of d^5 Fe^{3+} and d^3 Cr^{3+} this symmetry would then support X-ray magnetic circular dichroism. It is also worth noting that the crystal structure of this material is the same as that commonly associated with skyrmion lattices, and the observed ferromagnetic ordering is consistent with such behaviour.[60]

2D Magnetism

As highlighted by the early studies on $Cu(Fm)_2{\cdot}4H_2O$[32, 34-36] MOFs and coordination polymers are natural hosts for low dimensional magnetism due to their ability to contain strongly coupled magnetic chains and sheets. Where these motifs are well isolated they become suitable hosts for exotic low dimensional magnetism. Coupling between these low

dimensional motifs can, however, be larger than expected from simple inspection of a crystal structure, particularly for layered materials. One example of this is $Fe(NCS)_2(pyrazine)_2$, a MOF with only 2D extended connectivity, which adopts a 2D layered structure with $FeN_4(NCS)_2$ octahedra connected through the pyrazine into an essentially square lattice.[61] Physical property measurements are consistent with onset of an antiferromagnetic state near 6 K, with neutron powder diffraction studies on a deuterated sample suggesting this is an incommensurately modulate magnetic structure, with a **k**-vector of [1,0,0.27(1)], indicating a modulation in the magnetic structure that repeats ~3.7 unit cells along the *c*-axis. It was found to adopt a structure with nearest neighbour Fe cations coupled antiferromagnetically within the layers, with the magnitude of these magnetic moments varying sinusoidally between layers. Elastic and inelastic neutron measurements indicate a 2D Ising system and fits using a 2D square model to the heat capacity gave an excellent fit with a J_{intra}/k_B of 3.0 K.[61] Fits to inelastic neutron scattering, however, suggest interlayer coupling of J_{inter}/k_B of 1.5 K, surprisingly significant for a system with only through-space interactions between the layers; this may be partially explained by the interlayer Fe-Fe separation being only 7.2 Å *c.f.* to the 7.3 Å intrasheet distance.[61] Neutron spectroscopy indicates a spin gap of 1.64 meV with no noticeable spin-wave dispersion present in the ordered regime;[61] the magnetic excitation at 1.64 meV broadens and smoothly decreases towards large Q in the paramagnetic phase, which suggest that antiferromagnetic order of the layers is preserved locally well above the ordering temperature.

Another example of a 2D MOF are the metal malonates, $Na_2M(mal)_2{\cdot}2H_2O$ (M = Mn, Fe, Co, Ni or Cu, mal is malonate), which have 2D inorganic layers of MO_6 octahedra, connected via the carboxylate groups of the malonate ligands. These layers are stacked along the *c*-axis with Na atoms and water molecules located in the interlayer spacing,[62, 63] which should decrease the strength of interlayer coupling relative to intralayer coupling. Magnetic property measurements indicate that the Mn and Co frameworks are antiferromagnetic below 8 and 13 K, while the Fe and Ni MOFs are canted antiferromagnets below 16 and 24 K, respectively; the Cu compound has only very weak ferromagnetic interactions with magnetic order likely suppressed by all coupling pathways within the plane involving the Jahn-Teller elongated axis.[62, 63]

Neutron diffraction measurements on samples of the $Na_2M(mal)_2{\cdot}2H_2O$ compounds (30 atom % hydrogen) suggest long-range magnetic order in the four compounds in the family known to undergo antiferromagnetic transitions.[63] Observed magnetic scattering indexes on a **k**-vector of 0 and the structures, solved using representation analysis, all have nearest neighbour transition metals coupled antiferromagnetically through carboxylate groups (see Fig. 5). They vary, however, with regards to the spin orientation with the moments in the Mn and Ni compounds aligned along the *c*-axis and, therefore, perpendicular to the magnetic planes while the ordered spins of the Fe cations lie in these planes along the *b*-axis. $Na_2Co(mal)_2{\cdot}2H_2O$ is more complex with the spins offset 40° from the *c*-axis towards *b*-axis with the orientation of this rotation alternating between neighbouring layers leading to a non-collinear structure. The magnetic structures determined did not resolve the spin canting thought responsible for the small ferromagnetic component in the Fe and Ni-based compounds identified in magnetic property measurements; the *Pbca* magnetic symmetry these materials adopts does not allow for this so these must stem from a distinct irrep.

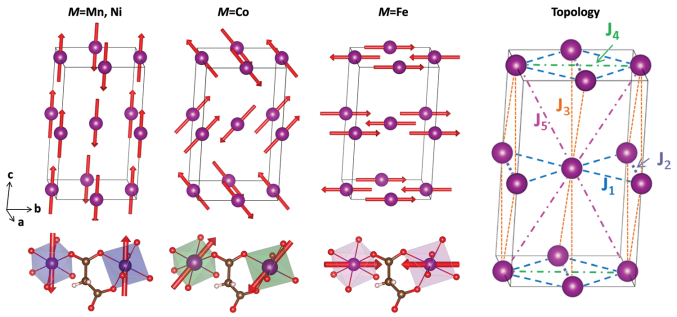

Fig. 5: Magnetic structures of the $Na_2M(mal)_2{\cdot}2H_2O$ frameworks, with the non-magnetic atoms omitted and coupling via carboxylate ligands shown separately below. The rightmost figure shows the possible magnetic coupling pathways in this material. Reproduced from Ref. 63 with permission from The Royal Society of Chemistry.

To obtain insight into the interlayer and intralayer magnetic exchange interactions from first principles in the $Na_2M(mal)_2{\cdot}2H_2O$ phases, DFT calculations based on the GGA+U exchange correlation functional were utilised.[63] The authors determined the values of U for the different divalent metal cations, using a self-consistent approach[27] on the experimentally determined low-T structures. With the Hubbard U values determined (U = 5.75, 5.85, 6.25 and 10.50 eV for Mn, Co, Ni and Cu respectively), the structures were subsequently relaxed to optimise the hydrogen positions. Magnetic exchange couplings up to 5th nearest neighbour (three of which are intralayer, the other two being interlayer) could then be calculated using a supercell of these relaxed structures with carefully chosen inequivalent spin configurations. As expected from the layered structure, the nearest neighbour intralayer coupling (J_4 in Fig. 5) was found to be largely dominant, and antiferromagnetic, except in the case of Cu which was ferromagnetic. Whilst the Ni malonate also had a dominant nearest neighbour intralayer coupling, the interlayer couplings were still very sizable (J_3 in Fig. 5 was ~7K) in qualitative difference to the other metal malonates, which were orders of magnitude smaller.

This combined neutron and DFT study suggest the $Na_2M(mal)_2{\cdot}2H_2O$ materials, with the exception of the Cu-containing compound, are essentially 2D antiferromagnets with only weak interlayer coupling between them and on that basis fits to the magnetic susceptibility properties of $Na_2Mn(mal)_2{\cdot}2H_2O$ were conducted using a Lines model for an antiferromagnetic square lattice;[63] this reproduced the nearest-neighbour coupling strength determined from DFT and the observed Curie-Weiss temperature of this material closely, confirming it is very close to a realization of a weakly coupled 2D antiferromagnetic square lattice. Equivalent analysis could

not be extended to other members of the series where there is some orbital contribution of the magnetic moment but their behaviour is likely similar.

Some MOFs have covalent bonding between layers but through a large ligand, which is commonly anticipated to lead to weak coupling between them. One example of this is the $M_2(OH)_2(tp)$ (where M is Mn^{2+}, Fe^{2+} or Co^{2+} and tp is tetraphtalate) family,[64] which feature two alternating edge-sharing chains of crystallographically distinct M cations connected by their corners to make a layered structure with layers pillared by the tetraphtalate ligands.[64] Magnetic property measurements suggested the onset of antiferromagnetic order at 39 K, 65 K and 48 K for the Mn, Fe and Co containing compounds, respectively.[64-66] The magnetic states of $Co_2(OH)_2(tp)$ are particularly complex, with an additional transition to a canted antiferromagnet observed at 45 K, the ferromagnetic component of which was suggested by alternating current (AC) susceptibility measurements to be dynamic in nature. A further transition involving a significant increase in the spin canting is observed above 3 kOe with the field required to cause this decreasing at lower temperatures and extrapolated to 0 kOe around 15 K.[64]

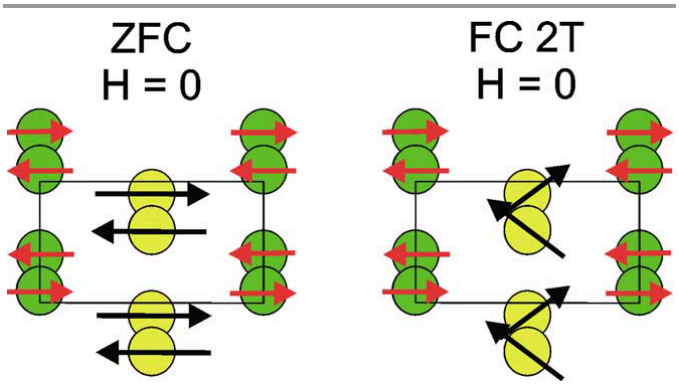

Fig. 6: Magnetic structure of two neighbouring layers in $Co_2(OH)_2(tp)$ after zero field cooling and 2 T field cooling. This shows the large spin canting that occurs under an applied field via rotation of the spin on the Co2 site (shown in yellow) while the spin on the Co1 site (shown in green) remains unchanged. Reproduced from R. Feyerherm, A. Loose, P. Rabu and M. Drillon, "Neutron diffraction studies of canted antiferromagnetic ordering in CoII hydroxide terephtalate" *Solid State Sci.*, 2003, **5**, 321-326.

Neutron diffraction measurements on a 0.5 g deuterated sample of $Co_2(OH)_2(tp)$ confirm antiferromagnetic order below 48 K.[67] This results in a structure with ferromagnetic chains coupled antiferromagnetically to each other both within and between the layers (see Fig. 6). No indication of canting in the weakly canting phase could be resolved, which is consistent with the ferromagnetic component not being long-range ordered. The magnetic moment of one of the distinct Co cations was larger than the other, *c.f.* 2.3 μ_B to 3.8 μ_B for Co1 and Co2, despite the magnetic moment evolution appearing fully saturated below 40 K.[67] This is likely a result of the magnetic moment of Co1 lying along the hard axis while Co2 has its moment aligned along its easy axis, suggesting the antiferromagnetic coupling is significantly stronger than single ion anisotropy. Analogous measurements of $Fe_2(OH)_2(tp)$ and $Mn_2(OH)_2(tp)$, carried out using hydrogenous samples (26 atom % H), show that their magnetic structures are very similar to that of $Co_2(OH)_2(tp)$, although the magnetic moments, which are all close to completely ordered, are oriented along the chain direction instead of perpendicular to it as in $Co_2(OH)_2(tp)$.[65, 66] A doped series of $(Co_{1-x}Fe_x)_2(OH)_2(C_8H_4O_4)$ investigated by Mesbah[66] showed partial cation ordering of the Fe^{2+} cation on the M2 site and magnetic structures in which the magnetic moments reorient from along the edge-sharing chains to perpendicular to them between 50 % Fe and 25 % Fe. The difference in ordered magnetic moment on the two sites opens up around the same time, confirming this is related to one being close to the easy axis and one being close to the hard axis of the Co-rich phases.

There was no observation of a transition to the strongly canted phase in zero field neutron diffraction studies of $Co_2(OH)_2(tp)$.[67] Patterns collected after cooling the sample in a 20 kOe field to 10 K, however, indicated the moments of the two distinct Co cations are no longer collinear; the moments in one of the chains of Co cations rotate from being perpendicular to the chain direction to canting 37° towards it while remaining approximately parallel to the sheets of CoO_6 polyhedra (see Fig. 6).[67] Importantly the antiferromagnetic correlations between layers is retained, suggesting these interactions are more significant than expected from a naïve view of the structure – likely because coupling across aromatic rings can be significant. That an applied field is required to observe this large canting suggests the weakly canted antiferromagnetic state is the ground state and the highly canted state only emerges as a result of applied magnetic fields; applying magnetic fields is an inherent part of a magnetometry measurement and bulk property measurements can thus can overlook such effects.

$Co_2(cbut)(H_2O)_3$ (cbut = 1,2,3,4-cyclobutane-tetracarboxylate) also features layers pillared by the backbone of the organic ligand but would be expected to exhibit more 2D-like behaviour because of the lack of aromaticity.[68] The complex layers of this material feature edge-sharing chains of distinct octahedral cobalt cations with Co2Co1Co1Co2 repeating units, with these chains connected to each other via carboxylate linkages through a third distinct Co site to form inorganic layers (see Fig. 7). Magnetic property measurements suggest Co cations interact ferromagnetically at higher temperatures before onset of long range antiferromagnetic order at 5 K. Applying fields greater than 1.5 kOe at 2 K leads to weak ferromagnetic order with a net magnetization slightly higher than one Co cation per mole.[68]

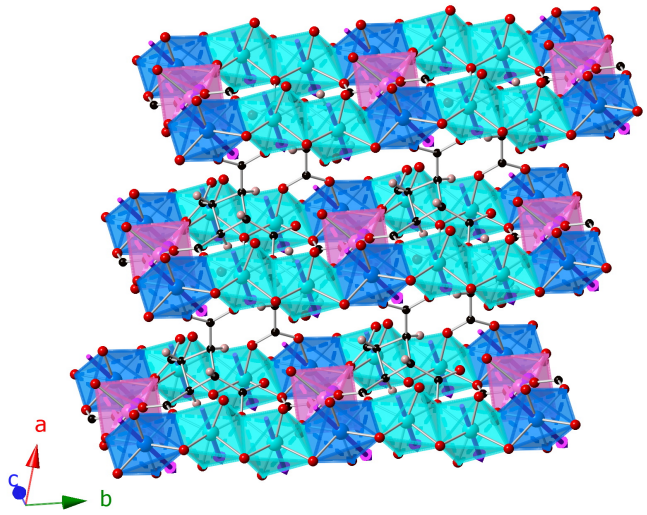

Fig. 7: Structure of $Co_2(cbut)(H_2O)_3$ showing edge sharing chains of octahedral Co1 (turquoise) and Co2 (dark blue) cations connected via Co3 (purple) cations with neighbouring chains bridged by the backbone of the ligand.[68] The spin orientations are shown as purple arrows. All other colours are as in Fig. 1.

The complex triclinic structure of $Co_2(cbut)(H_2O)_3$ makes it difficult to hypothesise where the combination of ferromagnetic and antiferromagnetic coupling required for this complex behaviour originates without direct examination. Investigation of the magnetic structure of this material using neutron powder diffraction collected on a hydrogenous sample (32 atom % hydrogen) indicated a **k**-vector of (½,0,0) i.e. a doubling of the magnetic unit cell length along the *a*-axis compared to the crystallographic unit cell.[68] The complex pattern obtained required fits be carried out against the difference between diffraction patterns above and below the magnetic ordering temperature to enable magnetic scattering to be reliably extracted from nuclear scattering; possible structures were tested as determined by representation analysis. At 2 K coupling within the edge-sharing chains was found to be ferromagnetic but the fully ordered Co2 spins offset from the incompletely ordered Co1 spins by around 10°.[68] Chains within a layer are aligned ferromagnetically through primarily antiferromagnetic coupling between the Co3 cations that connect neighbouring chains. This non-collinear magnetic structure is likely due to the strong anisotropy of Co leading to significant preferences for the local easy axis, which varies between the three distinct sites. Coupling between layers is antiferromagnetic and it appears likely that the suppression of this coupling by an applied magnetic field causes the metamagnetic transition as this would give the expected magnetization of about one Co(II) cation per mole; this significant difference in behaviour with applied field compared to the $M(OH)_2(tp)$ series is consistent with weaker interlayer coupling.

Linear dicarboxylate ligands, of the type $CO_2(CH_2)_nCO_2$, are also commonly associated with structures with well separated layers of metal cations bridged via the backbone of the ligand. One example of this with novel magnetic behaviour is Mn(succ) (succ is succinate), which adopts a unique structure built from two alternating layers with significantly different connectivity; one of which has a square lattice of corner-sharing MnO_6 octahedra while the other has edge-sharing chains of MnO_6 octahedra bridged by carboxylate groups (see Fig. 8).[69] Magnetic property measurements indicated an antiferromagnetic transition below 12 K, with a second phase transition observable in heat capacity data at 6 K. Neutron diffraction measurements, on a deuterated sample, revealed additional reflections consistent with a **k**-vector of (0,-0.5225,0) below 12 K with additional reflections observed below 6 K associated with a **k**-vector of (-1,0,1).[70] Using representation analysis it was determined that the correct model for the higher temperature magnetic state has ferromagnetic ordered edge-sharing chains, which couple antiferromagnetically to neighbouring chains while the spin of the corner-sharing layers remain disordered. The magnitude of the magnetic moments of the edge-sharing chains vary sinusoidally but remain tilted 40° from perpendicular to the layer.[70] The lower temperature magnetic phase is associated with ordering of the moments in the corner-sharing layer, with nearest neighbours antiferromagnetically coupled and moments tilted 15° from perpendicular to the layer.

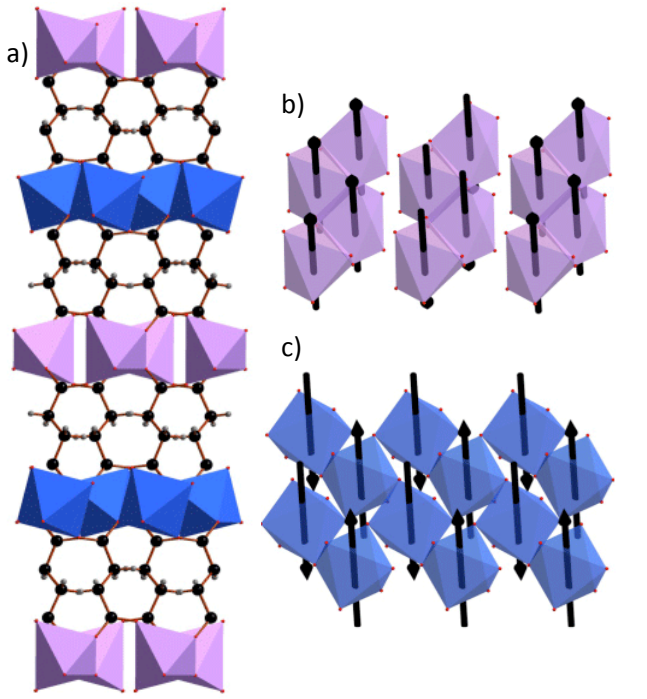

Fig. 8: a) Crystal structure of Mn(succ) showing its alternating layers of edge-sharing (pink) and corner-sharing (blue) MnO_6 octahedra.[70] The black arrows in b) and c) show the magnetic structures of these two distinct layers. All other colours are as in Fig. 1.

The transition to the second antiferromagnetic state in Mn(succ) does not appear to effect either the orientation or magnitude of the ordered magnetic moments of the edge-sharing layer, suggesting these are only very weakly coupled, as would be expected from their different **k**-vectors. The magnetic moments in both layers do not completely order to the lowest temperature examined and the magnetic

reflections associated with ordering of the edge-sharing layer are significantly broader than the other reflections, which is consistent with incomplete long-range magnetic order. Standard GGA DFT calculations indicated that the interlayer coupling is orders of magnitudes weaker than the intralayer coupling, consistent with a material close to the layered limit.[71]

A similar layered material, Co(adip) (adip is adipate), exhibits anisotropic thermal expansion as a result of its unusual magnetoelastic coupling.[72] This compound has planes of CoO_4 tetrahedra bridged by carboxylate groups within the plane and through the ligand backbone between them.[73] Magnetic property measurements indicate it is antiferromagnetic below 15 K, with powder neutron diffraction studies on a deuterated sample suggesting a magnetic structure with a **k**-vector of (0,½,0).[72] The magnetic structure has antiferromagnetic coupling between nearest neighbours within a plane with ferromagnetic alignment between adjacent layers (see Fig. 9); the magnetic moments are essentially fully ordered at 4 K and oriented perpendicular to the layers, likely a result of dipole-dipole coupling as tetrahedral Co^{2+} lacks any strong magnetic anisotropy.

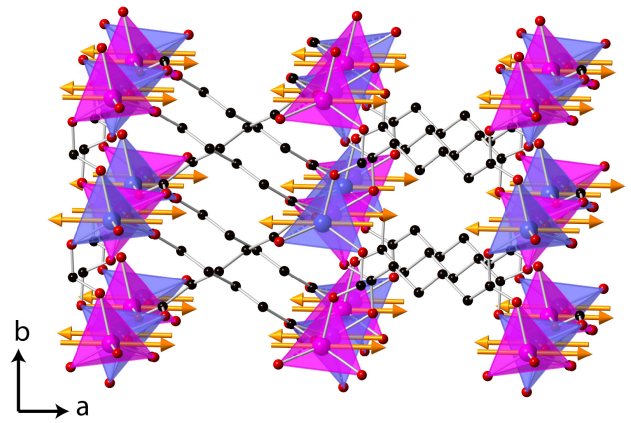

Fig. 9: Magnetic structure of Co(adip) with distinct colours used to highlight the polyhedral with different spin orientations, shown by orange arrows.[72] The H-atoms are omitted for clarity and all other colours are as in Fig. 1.

Near the magnetic ordering transition of Co(adip) the interlayer axis undergoes anisotropic negative thermal expansion while the layers expand at an increasing rate. This was attributed to magnetoelastic coupling, one of the first clear examples in MOFs, with the contraction of the inorganic layer on cooling near the Néel temperature likely driven by antiferromagnetic exchange striction.[72] The weaker dipole-dipole coupling between the layers then facilitates the relief of the resulting strain by allowing the structure to expand in this direction. Standard GGA DFT calculations suggest intralayer coupling is about two orders of magnitude stronger than interlayer coupling, again consistent with an essentially 2D magnetic material in which long range order only occurs at very low temperature.[74] Comparison between ferromagnetic and antiferromagnetic DFT models shows similar thermal expansion trends as observed between paramagnetic and antiferromagnetic phases, supporting the hypothesis that this is a result of magnetoelastic coupling.

1D Magnetism

As discussed in a number of the magnetic materials observed thus far chains are a ubiquitous motif in MOFs and coordination polymers. Such chains exhibit unique, often non-classical, magnetic states when isolated from interactions in other dimensionalities including entropy forbidding long-range magnetic order. One example of a coordination polymer with such interactions is orthorhombic $MnCl_2(urea)_2$, which has edge-sharing chains of octahedral Mn bridged by chloride anions along the *c*-axis, with urea bonded terminally in the axial positions.[75] The structure of $MnCl_2(urea)_2$ is unique as the chains do not stagger but, held in place by hydrogen bonding between the ureas, the Mn in neighbouring chains are in parallel planes along the *b*-axis. Magnetic susceptibility measurements suggest a transition to an antiferromagnetic state at 9 K; susceptibility measurements are well fitted by a Fisher model including a mean-field correction term giving J_{intra} = -1.9(1) K and J_{inter} = 0.1(1) K, suggesting the material hosts the most strongly coupled $MnCl_2$ edge-sharing chains and is close to the 1D limit.[75] The magnetisation below 1.5 K has a discontinuity at 28 kOe consistent with a metamagnetic transition and then increases linearly to around 200 kOe before saturating at 5.3(2) μ_B/atom, consistent with classical behaviour.

Neutron powder diffraction patterns of a hydrogenous sample (42 atom % hydrogen) of $MnCl_2(urea)_2$ revealed additional Bragg reflections below 3 K, determined to be magnetic in nature, which can be indexed on a **k**-vector of 0.[75] These features emerge at much lower temperature than expected from magnetic property data suggesting the material likely has short-range 1D order between 3 and 9 K. The magnetic structure has antiferromagnetic-coupled chains, with unusual nearest neighbour interchain ferromagnetic coupling. The spins are perpendicular to the chain direction with a magnetic moment of 4.06(6) μ_B at 2 K. Since Mn^{2+} has too high a spin to be expected to exhibit quantum behaviour, as confirmed by the high field magnetisation of $MnCl_2(urea)_2$, this reduced moment cannot be due to quantum fluctuations. Since the saturation value from high field magnetisation measurements are consistent with the value expected for Mn^{2+}, the metamagnetic transition at 28 kOe was ascribed to a portion of the Mn^{2+} spin density that has been delocalised onto the polarisable Cl^- at zero magnetic field, estimated as being 0.13 μB per Cl^-, transferring back to the cation.[75] Inelastic scattering measured at 1.6 K show a band of excitations between 0.4 and 1.1 meV, which broaden out on heating to 5 K.[75] Fitting this excitation band with a Heisenberg model enables J_{intra} to be determined to be -2.22(6) K, weak Ising-like anisotropy as -0.14(3) K and the strongest J_{inter} as 0.10(2) K, consistent with the Fisher model but with greater precision; this enables the unusual ferromagnetic interchain coupling to be confirmed.

Spin chains can also be isolated in structures with extended coordination bonding in 3D provided magnetic coupling is only strong along one-axis. A somewhat unexpected example of this are some members of the monoclinic $M(dca)_2pyz$ (dca –

dycanoamide and pyz – pyrazine) series.[76, 77] All late first row transition metals can be incorporated into this series, forming a doubly interpenetrated network with octahedral cations bridged into a pseudo-ReO_3 network, more commonly associated with 3D magnetism, by both pyrazine ligands, which occupy *trans*-position, and four equatorial [$N(CN)_2$] ligands (see Fig. 10). Only Mn and Cu phases undergo magnetic transitions above 2 K, at 2.7 K and 3.5 K, respectively, with 1D Heisenberg models fitting the susceptibility well and yielding J_{intra} of -0.27 K and -5.45 K, respectively.[76, 78] Pulsed field measurements show the magnetisation of $Cu(dca)_2pyz$ follows a concave curve that increases most rapidly as it saturates at 7.4 T, consistent with the behaviour expected for a quantum S=1/2 Heisenberg antiferromagnetic chain.[78] AC susceptibility and heat capacity measurements of $Mn(dca)_2pyz$ are consistent with the transition at 2.7 K being to a 3D ordered state.[79] In contrast muon spin spectroscopy indicates that $Cu(dca)_2pyz$ does not exhibit long range magnetic order above 0.02 K; on this basis and the J_{intra} extracted from fitting the susceptibility measurements J_{inter}/J_{intra} was estimated to be $1.43x10^{-3}$, one of the best realisations of an isolated spin-1/2 Heisenberg AFM chain.[78]

Extended Hückel molecular orbital calculations for $Mn(dca)_2pyz$ show the e_g energy levels are split with the dz^2 level 0.7 eV higher in energy, with these orbitals dominating the magnetic coupling within the Mn-pyrazine-Mn chains via σ-interactions;[79] coupling through the dicyanoamide linkers within the plane an order of magnitude weaker. DFT calculations using hybrid functionals for $Cu(dca)_2pyz$ showed a large difference in the spin density in the pyrazine linkage between the broken-symmetry and high-spin states but not the dicyanoamide linker, consistent with the magnetic coupling through the pyrazine ligand being about 50 times stronger than through the dicyanoamide ligand, qualitatively consistent with values extracted from physical properties and muon spin measurements.[78] The more purely 1D magnetic state in $Cu(dca)_2pyz$ is likely at least partially a result of its cooperative Jahn-Teller distortion having its long axis oriented towards dicyanoamide ligands, alternating orthogonally between successive octahedra, weakening its intraplane coupling further.[78]

Powder neutron diffraction measurements on a deuterated sample of $Mn(dca)_2(pyz)$ revealed additional reflections below the magnetic phase transition, indexed on a **k**-vector of (0.5,0,0.5).[79] The magnetic structure was determined to feature nearest neighbour antiferromagnetic coupling both within the chains and between them, with the two interpenetrating lattices being aligned ferromagnetically; spins are oriented at a 45° angle from the chain direction (see Fig. 10).[79, 80] The rate of decay in the intensity of the strongest magnetic reflection is consistent with that expected for a 3D Heisenberg antiferromagnet and magnetic diffuse scattering was observed between 2.7 K, the Néel temperature, and 15 K, consistent with short-range correlations within the chains of the material remaining in the paramagnetic state.[81] Neutron diffraction studies of $Cu(dca)_2pyz$ were not carried out, because in the absence of a 3D ordered ground state conventionally large single crystals are required to interpret the diffuse scattering associated with low dimensionally ordered states. Inelastic neutron spectra were, however, measured for both compounds below 2 K with features attributed to magnetic spin waves in quasi-one dimensional materials at 0.23 meV and 0.4 meV in $Mn(dca)_2(pyz)$ and $Cu(dca)_2(pyz)$, respectively; this is consistent with the stronger 1D magnetic coupling in the latter.[78, 81]

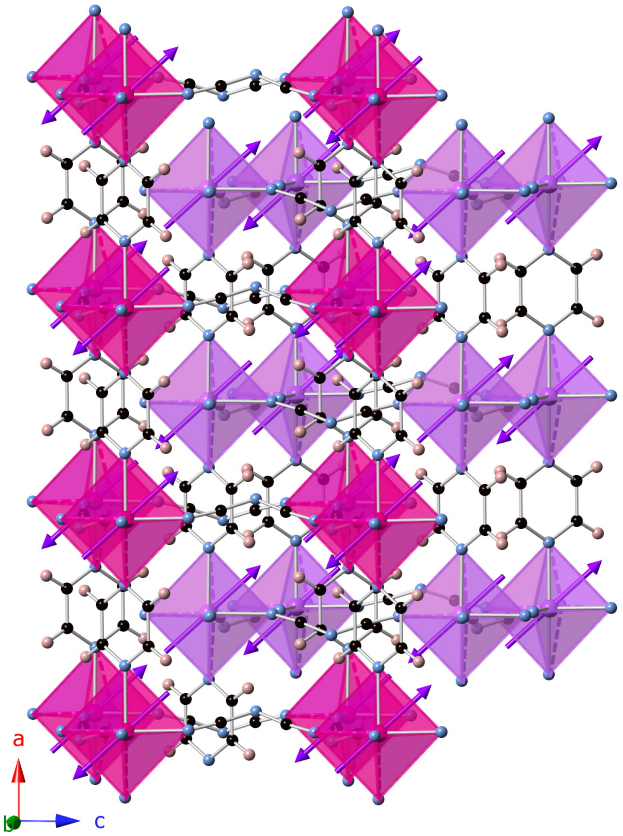

Fig. 10: The structure of $Mn(dca)_2(pyz)$ with the MnO_6 polyhedra in the two interpenetrated networks shown in pink and lavender and spin orientations shown in purple.[79] All other colours are as in Fig. 4

Ising spin chains, incorporating strong anisotropic metal cations, are of particular interest as they represent the simplest magnetic chains in which spins can only point up or down. Although entropy still forbids long-range magnetic order in isolated Ising spin chains at any realizable temperature, they lack the very low energy (gapless) excitations associated with Heisenberg chains that prohibit order at 0 K.[82] One example of this class of spin chains is $Co_4(OH)_2(seb)_3$ (seb is sebacate), which adopts a monoclinic structure with corner sharing zig-zag chains of slightly distorted CoO_6 octahedra (Co1) interconnected with trigonal bipyramids (Co2) into a complicated double chain structure (see Fig. 11);[83] these chains are bridged in the other two directions by the long sebacate ligand leading to an interchain separation of 1-2 nm. Magnetic property measurements reveal a transition to a weak ferromagnetic phase near 5 K, with magnetisation measurement showing an initial rapid rise before levelling off to antiferromagnetic behaviour.[83] Heat

capacity measurements suggest this transition is to a long range ordered state while AC susceptibility measurements show significant frequency dependence consistent with single chain magnets, with an energy barrier of 67 K and characteristic time of 1.4×10^{-11} s, within the 3D order state. Detailed analysis reveals thermal dependence consistent with a predominately 1D Ising system and a large distribution of relaxation processes not typical of the single-spin processes in single chain magnets attributed to the existence of broad domain walls.

Neutron powder diffraction measurements were obtained from a hydrogenated sample (51 atom % H) of $Co_4(OH)_2(seb)_3$ and the magnetic structure analysed from temperature-subtracted data.[84] All magnetic reflections were indexed on a structure with a **k**-vector of 0 and representation analysis was used to determine the possible magnetic structures. The magnetic structure was determined to have octahedral Co cation spins aligned parallel to the chain while those of the Co in the trigonal bipyramids are tilted from the chain axis by 35° resulting in a non-collinear structure (see Fig. 11).[84] The moments of the octahedral cations lie close to the equatorial plane while those of the trigonal bipyramids are canted further out of their equatorial plane, as commonly observed for strong anisotropy in this coordination environment. Nearest-neighbour octahedral cations are antiferromagnetically coupled to each other while the square pyramidal Co cations are ferromagnetically coupled to the octahedral Co cations with which they share an edge. The magnetic moment of the square pyramidal Co cations along the chain direction are opposed by those on the opposite side of the chain but the components perpendicular to the chain direction are uncompensated. As spins in neighbouring chains have the same orientations this is the origin of the weak ferromagnetic properties of this material.

The net magnetisation per Co cation in the magnetic structure of $Co_4(OH)_2(seb)_3$ is 0.82 μ_B, which is consistent with the magnetisation jump observed at very low applied fields being caused by this net magnetisation being aligned with the magnetic field.[83, 84] Neutron diffraction patterns were also collected in an applied field, with the sample immersed in deuterated isopropanol, which freezes at low temperature to form a glass to fix the grains of sample in place.[84] The patterns did not show any obvious sign of a magnetic phase transition up to 2 T but relative temperature intensities of the reflections relevant to the spin canting in the chains suggestive of significant rearrangements of the spins were noted but the restricted data quality prevented detailed analysis. Diffuse magnetic scattering was seen in 0.5 and 2 T fields up to 10 and 13 K, indicative of the persistence of interchain correlations well above the Néel temperature.

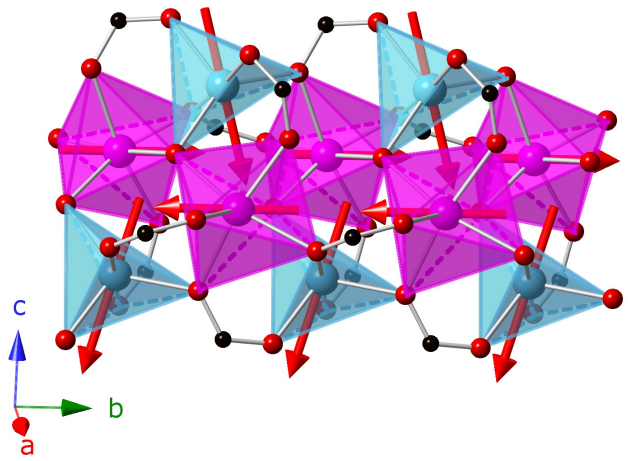

Fig. 11: The structure of the chains in $Co_4(OH)_2(seb)_3$ highlighting their trigonal bipyramids (blue) and octahedral (pink) Co and the spin orientations of these sites (red arrows).[84] All other colours as an in Fig. 1.

The spin chains discussed so far all have an odd number of unpaired electrons with the presence or absence of low energy magnetic excitations depending on whether they feature Ising or Heisenberg behaviour. In systems with an even number of electrons it is expected that there are no very low energy excitations, even for a Heisenberg system, because of nonlinear quantum fluctuations in the ground state.[82] This is the so-called Haldane gap, which contributed to Duncan Haldane being awarded a share of the 2016 Nobel prize. This gap can be closed in an applied field leading to a quantum phase transition at critical field H_c, from a quantum spin liquid phase to a long-range ordered structure at 0 K.[85] S=1 Ni^{2+} containing compounds are typically of most interest for studying such behaviour with the $Ni(dadp)_2N_3X$ (where dadp – 1,3-diamine-2,2-dimethylpropane and X = ClO_4 or PF_6) the first examples of closing the Haldane gap. These compounds, which are both monoclinic below room temperature, have octahedral Ni cations connected by the azide ligand with two bidentate amine ligands binding in *cis*-positions.[86, 87] These chains run along the *c*-axis and are well separated from each other by the bulk of the amine and the counteranion. Bulk magnetic property measurements indicate broad antiferromagnetic cusps near 35 K and 80 K for PF_6 and ClO_4 compounds, respectively; susceptibility measurements are well fitted by 1D Heisenberg models with J_{intra} of -27.9 K and -70.6 K. For $Ni(dadp)_2N_3ClO_4$ heat capacity measurements suggest a transition to a long range ordered state as associated with closing the Haldane gap at 116 kOe when the field is applied parallel to the chain direction;[87] in $Ni(dadp)_2N_3PF_6$ the gap appears to close around 48 and 60 kOe, depending on whether the field is applied parallel or perpendicular to the applied field.[88]

Neutron diffraction of deuterated samples of these materials allowed the microscopic nature of these high field ordered states to be observed, with single crystals used to make quantitative studies in applied fields attainable. $Ni(dadp)_2N_3PF_6$ showed commensurate spin ordering at 0.25 K, which is either true 3D order or quasi-2D short range order

depending on whether the magnetic field is aligned close to parallel or perpendicular to the chain direction (see Fig. 12 for a phase diagram).[89] Consistent with heat capacity measurements 3D order occurs at an applied field of 48 kOe when the field is applied along the $[1, \bar{1}, 0]$ axis while for field orientations perpendicular to the chain direction two-dimensional order within the *bc* plane is observed for fields above 60 kOe. In both cases the spins are perpendicular to both the chain direction and the applied field indicating the antiferromagnetic coupling is much stronger than the applied field strength.[89] In the 3D ordered state nearest neighbour chains, along the *b*-axis, are coupled antiferromagnetically but chains separated along the *a*-axis are ferromagnetically coupled while in the 2D ordered state there is no order along the a-axis; the large separation between chains in this direction and the weaker dipole-dipole coupling this results in appears to be strongly influenced by the direction of applied magnetic field. Studies on $Ni(dadp)_2N_3ClO_4$ have been more restricted because the critical field required to achieve a 3D ordered state, even at 70 mK, is much higher; 130 kOe with the field close to parallel to the *c*-axis axis.[88]

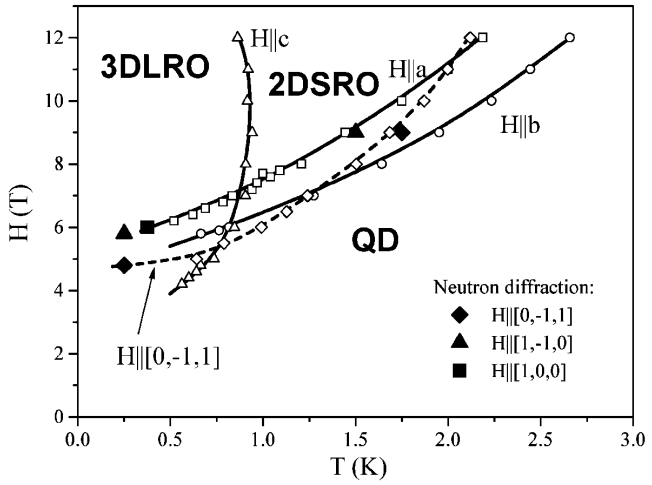

Fig. 12: Magnetic phase diagram of $Ni(dadp)_2N_3PF_6$ as a function of temperature and applied field along a given direction. QD, 2DSRO and 3DLRO stand for quantum disordered, 2D short range order and 3D long range order, respectively. Reprinted figure with permission from Y. Chen *et al.*, *Phys. Rev. Lett.*, **86**, 1618, 2001. Copyright 2001 by the American Physical Society.

Later neutron inelastic studies confirmed the onset of 3D magnetic order in $Ni(dadp)_2N_3PF_6$ above 120 kOe even when the applied field is perpendicular to the chain direction.[90] They also showed that the Haldane gap disappears around the same field strength at which 2D order emerges – 60 kOe. Furthermore, because these measurements were at 2.5 K, high enough to thermally suppress coupling between the chains, the observation of relatively sharp quasi-elastic features suggests that even in the absence of intrachain coupling quasi-long range 1D order emerges in the chains at high magnetic fields. This supports complete one-dimensional magnetic order within the chains at 0 K even in the theoretical absence of inter-chain coupling. Most recently it has been shown that, where the magnetic field is applied close to the chain directions, there is a narrow regime where only half the chains in the structure order magnetically.[91] This demonstrates that the field required to close the Haldane gap is highly dependent on local anisotropy that can only be probed through techniques that examine the atomic scale, rather than bulk anisotropy measured by macroscopic techniques. This also highlights that at low temperatures the interchain coupling only plays a small role in determining the transition field required to support long-range magnetic order and primarily suppresses spin fluctuations at 0 K that would otherwise destroy long-range 1D order. It also confirms there is likely plenty of room for further investigation of closing the Haldane-gap in the understudied $Ni(dadp)_2N_3ClO_4$ using modern high field magnets.

Spin Ladders

Spin ladders, which have spin chains with regular links between them are also of interest as the interface between 1 and 2D magnetism. A complex example of spin ladder type behaviour in a MOF is found in $Mn_2(OH)_2(sq)$ (where sq is squarate), which has a monoclinic zig-zag-like structure consisting of edge-sharing chains of MnO_6 octahedra, which are bridged into a ladder structure by a μ_3-coordinated hydroxide cation;[92] Mn cations in the rails are staggered by half the Mn-Mn separation along a ladder leading to two rung connections for each Mn. The squarate ligands, which stack along the ladder-direction, connect to six Mn from four different ladders. $Mn_2(OH)_2(sq)$ was originally reported to be a canted antiferromagnet below 32 K[92] but a powder neutron diffraction study of a deuterated sample showed that it adopts an antiferromagnetic structure with **k** = (0.5,0.5,0.5); this only emerges around 12 K suggesting the transition at 32 K is caused by the presence of a $MnCO_3$ impurity, which could be identified in the neutron patterns.[93] Bulk magnetic property measurements are notoriously influenced by even small ferromagnetic or weak ferromagnetic impurities, whereas magnetic structure determination by neutron diffraction is much less so.

Following testing of models of $Mn_2(OH)_2(sq)$ proposed by representation analysis it was established that the magnetic structure has antiferromagnetic coupling within the rails of a ladder and alternating antiferromagnetic and ferromagnetic rung coupling.[93] This is enabled by having three crystallographically distinct Mn-O-Mn bridges in the ladders with slightly different bond distances and angles. These distortions removed the frustration that would otherwise be imposed with this geometry in the case of equilateral symmetry with the ferromagnetic correlations occurring between Mn expected to have the weakest coupling on geometrical grounds.

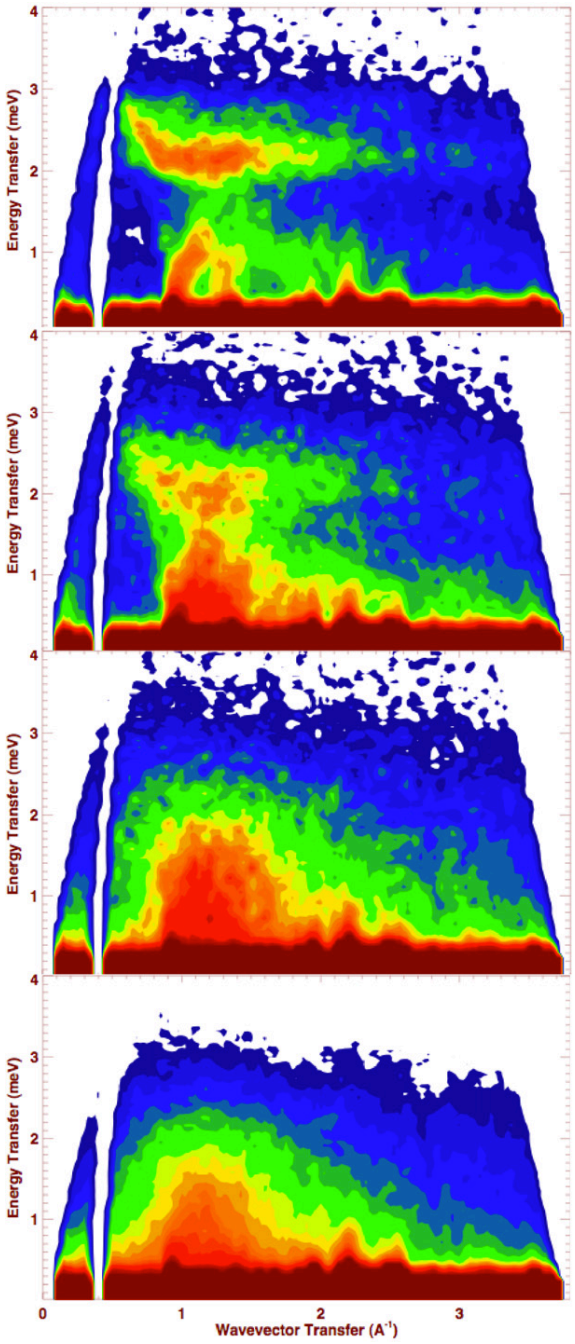

Fig. 13: Inelastic neutron scattering from $Mn_2(OH)_2(sq)$ collected at 5, 12, 20 and 40 K (top to bottom) shown as false colour plots. These show the temperature evolution of excitations centred at 1.2 meV and 2.2 meV in the 5 K data; these features show significant and restricted energy dispersion respectively. ©IOP Publishing reproduced with permission from reference 95. All rights reserved.

Broad features in neutron diffraction patterns are observed above the transition at 12 K in $Mn_2(OH)_2(C_4O_4)$, consistent with short-range magnetic correlations.[93] This is supported by muon spin measurement, which show a gradual decrease in symmetry below 50 K, consistent with the gradual development of short range magnetic order before symmetry decreases rapidly at 12 K, consistent with the onset of long range magnetic order only below this temperature.[94] Inelastic neutron spectroscopy indicates two excitations centred at 1.2 meV and 2.2 meV at 1.5 K (see Fig. 13).[95] As temperature increases the lower energy mode shifts to lower energies and broadens to merge with the elastic line by 12 K while the higher energy mode changes little below the 3D ordering temperature before broadening significantly a few degrees above it and then disappearing in the very broad low temperature mode by 25 K. The low energy mode shows dispersion in the measurements below 5 K meeting the elastic line at Q of 1.0 and 1.35 $Å^{-1}$, allowing it to be assigned as acoustic magnons that highlight the 1D nature of the system.

The more restricted dispersion and form factor dependence of the higher energy mode in $Mn_2(OH)_2(sq)$ resembles that expected from a spin dimer; its cross-section intensity versus Q is well fitted by a coupled Heisenberg ladder model with intraladder distances that agree well with the crystal structure and a $J_{intraladder}/J_{interladder}$ of -6.3(3).[95] The presence of this excitation well above the ordering temperature and its strong resemblance to a pairwise interaction between spins above 15 K suggests this is a singlet-triplet excitation enabling $Mn_2(OH)_2(C_4O_4)$ to be identified as a valence bond solid.[95] Between 25 K and 50 K Q-dependence of the entire inelastic region is well fitted by the singlet triplet excitations between spins, consistent with a transition to a valence bond liquid. This analysis points to this S=5/2 system showing quantum behaviour, not previously observed in a material with such large S values, attributed to the systems combination of low dimensional magnetism and geometric frustration.

Frustrated Magnetism

Magnetic frustration typically emerges when materials have several different competing interactions that cannot be simultaneously satisfied leading to competition between a variety of similar low energy states preventing a single ordered ground state emerging.[6] This leads to unique magnetic phenomena such as magnetic monopoles in spin ice[96] and spin liquids,[97] whose resonating spin pairs provide models for electron coupling in superconductors. While it might be naively thought that competing magnetic coupling in complex MOFs might make them ideal for such behaviour, often the structures adopted by these materials have low symmetry so the competing interactions are inequivalent enabling the stronger ones to win out and stabilize a ground state, at least at sufficiently low temperatures.

The partially frustrated spin ladder $Mn_2(OH)_2(sq)$ discussed above is one example where inequivalent interactions helps to relieve frustration; related $Co_3(OH)_2(sq)_2{\cdot}xH_2O$ (x = 0-3) is another in which both differences between hydrated and non-hydrated states emerge[98]. This material also exhibits unique idle spin behaviour in which, due to frustration, some of the spins in the material remain disordered when an ordered structure initially emerges before ordering at lower temperatures.[99] $Co_3(OH)_2(sq)_2{\cdot}3H_2O$ has a monoclinic structure based on brucite-like $Co_3(OH)_2$ buckled ribbons along the *c*-axis with the OH groups bridging isosceles triangles of Co atoms that connect to each other by either their edge or corner in an

alternating fashion (see Fig. 14);[100] these triangles are isosceles rather than equilateral lowering the potential frustration somewhat. There are two distinct distorted octahedral Co sites, Co1, which lies at the shared vertex of two triangles and Co2, with double the multiplicity, at the shared edge of two triangles. Each ribbon is connected to four others through squarate ligands creating lozenge-shaped channels occupied by water molecules, which can be removed on heating.[98] Magnetic property measurements of $Co_3(OH)_2(sq)_2{\cdot}3H_2O$ suggested an antiferromagnetic transition at 8 K followed by a transition to spin canted antiferromagnet at 6 K with glimpses of a third magnetic transition around 3 K while dehydrated $Co_3(OH)_2(sq)_2$ appears ferromagnetic below 8 K; AC measurements suggest both materials retain some magnetic dynamics in their ordered phases.[98, 99] Superexchange pathways are all close to 90° and, on this basis, ferromagnetic coupling within the ribbons was naively anticipated. Since intrachain coupling pathways change by less than 2 % during dehydration Kurmoo *et al*.[98] proposed that the transition from antiferromagnetic to ferromagnetic behaviour on dehydration is caused by changes in very weak inter-ribbon coupling.

Neutron powder diffraction patterns of deuterated $Co_3(OH)_2(sq)_2{\cdot}3H_2O$ reveal that the coupling within chains is principally antiferromagnetic in nature rather than the ferromagnetic coupling assumed on a geometric basis.[99] More specifically it reveals a complex incommensurate magnetic phase appearing at 8 K, replaced by other peaks appearing below 6 K, with further changes in intensity near the transition at 3 K. The lowest temperature magnetic phase has a doubled *c*-axis and, using the possibilities suggested by representation analysis, the magnetic structure was determined to have Co2 magnetic moments on the base of a triangle ferromagnetically coupled with moments perpendicular to the ribbon direction; these couple antiferromagnetically to those Co2 cations in the next triangle of the ribbons (see Fig. 14). The Co1 cations have moments aligned parallel to the ribbon and are antiferromagnetically coupled to the nearest neighbour Co1 cations. The perpendicular spin orientation of Co1 and Co2 cations minimizes the frustration between a Co1 cation and the Co2 cations in the two triangles of which it joins, to which it cannot simultaneously antiferromagnetically couple to in a collinear structure.

In the intermediate temperature magnetic phase the Co1 cations disorder, the first so-called idle spin behaviour associated with magnetic frustration in a structure with more than one site that then goes on to have all sites ordered at lower temperatures.[99] The symmetry of the ordering of Co1 and Co2 cations is different, which along with their different ordering temperatures, suggests that the coupling energies between the two Co sublattices is much weaker than their single ion anisotropy.[99] The larger separation between Co1 cations is likely the reason order on this sublattice is lost first; the presence of disordered spins alongside ordered Co2 cations may be the cause of the magnetic dynamics associated with magnetic order in this material. The highest temperature ordered magnetic phase is incommensurately modulated in two different directions.[99] While this is too complex to be reliably solved from powder diffraction it also belies previous thoughts that the transition at 6 K may involve a simple canting of this higher temperature phase, an easy interpretation to draw from magnetic susceptibility measurements. Single crystal neutron scattering could be used to solve the magnetic structure of the modulated phase but this is not possible in this case as only very small single crystals are available.

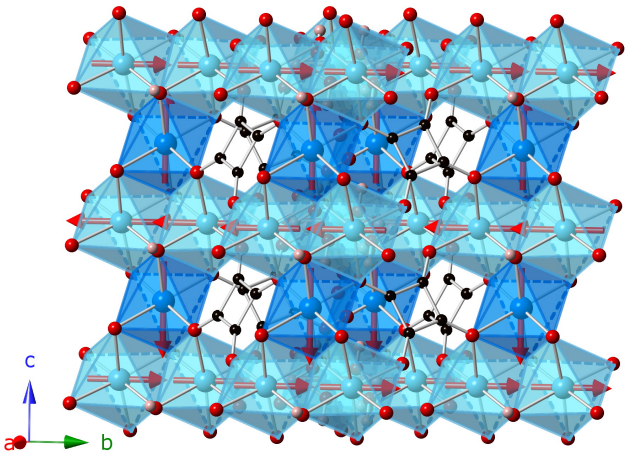

Fig. 14: Structure of $Co_3(OH)_2(sq)_2{\cdot}3H_2O$ in its lowest temperature ordered magnetic phase.[99] The Co1 and Co2 cations are shown in dark blue and turquoise, respectively, with their spin orientations in red. The water molecules are omitted for clarity and all other colours are as in Fig. 1.

Neutron diffraction patterns of dehydrated $Co_3(OH)_2(sq)_2$ reveal the presence of magnetic Bragg peaks below 8 K with additional peaks observed below 6 K.[101] These two phases were determined to be equivalent to the two commensurate phases observed in $Co_3(OH)_2(sq)_2{\cdot}3H_2O$, except that in the lower temperature phase the coupling of the intra-chain Co1 is ferromagnetic. That the ferromagnetic behaviour of $Co_3(OH)_2(sq)_2$ emerges from a structure with antiferromagnetic coupling in the ribbons is in sharp contrast with the hypothesis of Kurmoo *et al*.[98] based on magnetic property measurements while remaining fully consistent with the behaviour they observed. Such insight could only be gained by studying magnetic MOFs at a microscopic level. The change from antiferromagnetic to ferromagnetic coupling within the $Co_3(OH)_2$ ribbons is likely a result of the dominance of single ion anisotropy, which it is well established can be changed significantly by small distortions in the crystal field. Consistent with this the ordered magnetic moment at low temperature increases on dehydration from 4.00 to 5.2 μ_B for Co1 and 3.47 to 3.83 μ_B for Co2, suggesting a significant change in the *g*-value for Co1 from 2.7 to 3.5.[101] Mole *et al*.[101] contribute the absence of the modulated magnetic state in $Co_3(OH)_2(C_4O_4)_2$ to a larger difference between the strength of the single ion anisotropy and magnetic coupling strength; these are proposed to be similar in energy in the hydrated state and their competition leads to the emergence of an incommensurate phase.

Inelastic neutron scattering data collected on $Co_3(OH)_2(sq)_2$ showed no low energy excitations in the fully ordered

magnetic phase but in the idle spin phase a strong magnetic feature was observed at 1.18(2) meV.[102] This persists to temperatures well into the paramagnetic phase, broadening significantly. Fits to the *Q*-dependence of this excitation shows it is likely due to the interaction between the idle spin and the Co2 dimers, as it does not involve a change in overall magnetic moment.[102] This indicates that thermal energies equivalent to 3.4 K are required to break the interactions between Co1 and Co2 cations consistent with the observed transition temperature into the spin idle phase. The sharpness of this feature in the spin idle phase is likely due to the lack of spin fluctuations of the Co2 cations, while its persistence above the ordering temperature reveals substantial short-range spin correlations are maintained up to at least 75 K.

The $M(tca)_2$ (tca – tricyanoamides) are another family of magnetically frustrated MOFs based on stacked rows of triangles. This family adopts an interpenetrated orthorhombic rutile-like structure containing triangles of cations connected by the same ligand with antiferromagnetic interactions between them but with two cations in a triangle bridged by two ligands leading to doubly bridged chains along the *a*-axis.[103] Heat capacity and magnetic property measurements suggested the onset of 3D ordered phases at 1.2 K in $Mn(tca)_2$,[104] 3 K in $Fe(tca)_2$ with a further transition below 2 K,[105] and in Jahn-Teller distorted $Cr(tca)_2$ at 6.1 K;[106] the bulk measurements do not reveal the extreme magnetic frustration present in $V(tca)_2$, which has a frustration index of over 40.[106]

The relative strength of the intrachain interactions increases on going from Mn to Fe to Cr, reducing frustration and leading to interesting changes in their magnetic structure.[104, 105] For $Mn(tca)_2$, where the relative strength of interchain and intrachain coupling is the most similar and therefore frustration is strongest, powder neutron diffraction patterns indicate a magnetic **k**-vector of (0.3111(5), 0.5, 0); with magnetic reflections best fitted by a structure with XY-like antiferromagnetic triangles with spins offset by around 112°, indicating significant competition between magnetic interactions in this material (see Fig. 15).[104] This state can be interpreted as having doubly bridged chains with an antiferromagnetic spiral spin structure and about 70 % of the magnetic moment of the Mn cation ordered. The field dependence of the magnetic reflections suggests transitions to states with triangles with two spins up and the other down at 13.5 kOe and a spin-flopped 2-1 spin phase at 16 kOe (see Fig. 16), these remain incommensurate indicating that applied field does not lift frustration in $Mn(tca)_2$ when the effects of fields cause spin reorientation.[104]

In contrast with $Mn(tca)_2$ neutron diffraction patterns indicate that both magnetic phases in $Fe(tca)_2$ have collinear antiferromagnetic coupling within their doubly connected chains.[105] The higher temperature ordered phase has a **k**-vector of (0.530(5), 0, 0), with moments lying close to the easy axis along the [0,1,1] direction. The magnetic moments vary sinusoidually along the chain direction with a maximum of 3.4(1) μ_B. In the lower temperature phase, which is not modulated, the interaction between nearest neighbour chains switches from ferromagnetic to antiferromagnetic coupling and the moments rotate so they are aligned significantly closer to the *c*-axis. The greater anisotropy of Fe and the stronger intrachain coupling appears to somewhat lift frustration, allowing this commensurate order, but since either temperature or an applied field of 18 kOe leads to an incommensurate phase the effects of competition between magnetic interactions is clearly not removed completely. In $Cr(tca)_2$ the Jahn-Teller distortion is oriented perpendicular to the chains causing relative coupling within the chains to be even stronger.[106] Magnetic reflections in powder neutron diffraction data index on a **k**-vector (0.5, 0.5, 0) with antiferromagnetic coupling within the doubly bridged chains; all magnetic moments are fully ordered and aligned along the *c*-axis showing none of the magnetic modulations indicative of frustration in either $Mn(tca)_2$ and $Fe(tca)_2$.[106]

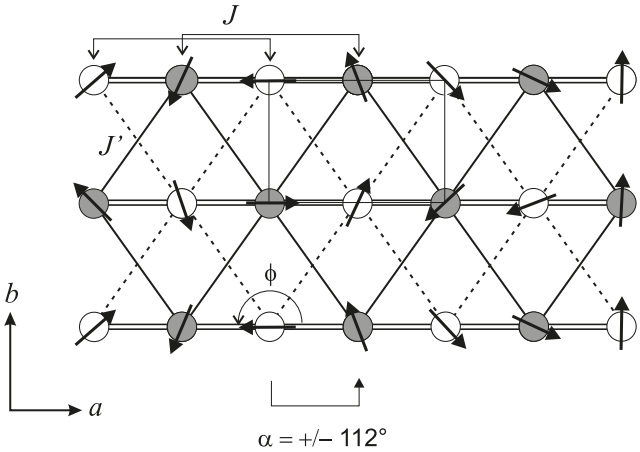

Fig. 15: The zero field incommensurate magnetic structure of $Mn(tca)_2$ with doubly bridged chains shown as double lines and the cations in the two interpenetrated networks shown as filled and opened spheres. ©IOP Publishing reproduced with permission from reference 104. All rights reserved.

The effect of symmetry lowering on relieving the magnetic frustration inherent in this lattice is also indicated by the $M(dca)_2$ (dca – dycanoamide) where the doubly bridged chains are instead coupled through the central N of the ligand.[107, 108] These compounds all magnetically order at significantly higher temperatures than their $M(tca)_2$ analogues and do not show any signs of magnetic frustration due to ferromagnetic coupling within their chains.[107, 108] They do demonstrate an interesting alternation between antiferromagnetic and ferromagnetic coupling between their chains depending on whether the incorporated transition metal has more of less than six *d*-electrons. This was initially attributed to an increasing superexchange angle with decreasing cation size, with a critical crossover angle of 142.0(5)°,[108] but more recently standard GGA DFT calculations have suggested that this is a small effect and *d*-orbital occupation is the more significant factor.[109]

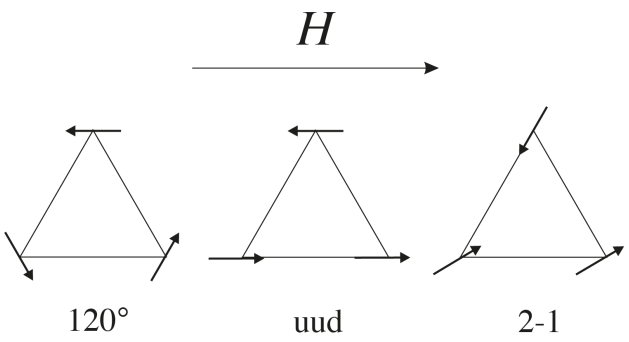

Fig. 16: Evolution of the order within the frustrated triangles in $Mn(tca)_2$ magnetic phases with increasing applied field from that found in an idealised spiral structure to an up-up-down (uud) arrangement as a spin-flop like 2-1 phase. ©IOP Publishing reproduced with permission from reference 104. All rights reserved.

Thus far the frustrated and low dimensional materials discussed in this article from which detailed insight has been gleaned from neutron diffraction have all been found to adopt a 3D ordered magnetic structure at low temperatures; this allows insight into how order is achieved through either having sufficient interactions between their low dimensional motifs or having frustrated interactions with inequivalent coupling strength such that complex ordered magnetic structures emerge as a compromise between conflicting interactions. As seen in $Cu(dca)_2pyz$[78] and, possibly, $V(tca)_2$[106], some low dimensional and frustrated coordination polymers and MOFs are likely to avoid such conventional long range order at any realizable temperatures. Conventionally the magnetic structures of such materials have been less accessible using neutron diffraction, required to support further computational and inelastic scattering studies, in the absence of large single crystals rarely available from framework materials.

Recently a new method based on reverse Monte Carlo (RMC) fitting to diffuse magnetic scattering from powder data has been developed by Paddison *et al.*[110] that allows the local magnetic structure of such materials to be probed. Thus far this approach has only been applied to one published MOF, $Tb(Fm)_3$.[111, 112] This belongs to a family of $Ln(Fm)_3$ (*Ln* = lanthanide) in which the LnO_9 polyhedra form face-sharing chains packed into a triangular lattice, with interchain coupling through the formate ligand. In the context of their magnetic properties this family first attracted attention as magnetocaloric coolants, which are comparable to the benchmark oxides for such applications at low applied magnetic fields.[5] $Tb(Fm)_3$ is particularly interesting as although its peak magnetocaloric entropy change is less than $Gd(Fm)_3$ its peak is observed around 4 K. This potentially shifts the useful temperature range these materials can be used to the regime where large amounts of liquid helium are needed for e.g. superconductors in NMR and MRI instrumentation.[112] This appears to be a result of the greater ease of magnetization of $Tb(Fm)_3$ in low fields, which is unusual because of the greater magnetic anisotropy of Tb compared to Gd.

Neutron diffraction was carried out on $Tb(Fm)_3$ to probe its magnetic structure, with magnetic reflections observed below 1.6 K being assigned to a **k**-vector (0,0,1).[112, 113] These were initially interpreted as indicating 3D magnetic order and, of the possible structures suggested by distortion mode analysis, two provided equally good fits to the observed data. Both of these feature ferromagnetically coupled chains with moments parallel to the chain direction; they differ in that one has two of the chains in a triangle coupled ferromagnetically to each other with half the ordered moment of the third antiferromagnetically coupled chain, while the other possible structure has two chains in each triangle coupled antiferromagnetically to each other with the third remaining disorded, a Partially Disordered Antiferromagnet (PDA) (see Fig. 17).[112, 113] In either case the ferromagnetic coupling within the chains could explain the magnetocaloric properties of $Tb(Fm)_3$, as opposed to $Gd(Fm)_3$ where this is thought to be antiferromagnetic[5]. Such ferromagnetic correlations are confirmed to be retained in the paramagnetic state, the regime of interest for magnetocaloric properties, by RMC fits to diffuse scattering using an Ising-like refinement with magnetic moments parallel to the chain direction; this yielded an intrachain ferromagnetic correlation length of 9.2(1.3) Å at 3 K and very weak antiferromagnetic correlations between these chains.[112]

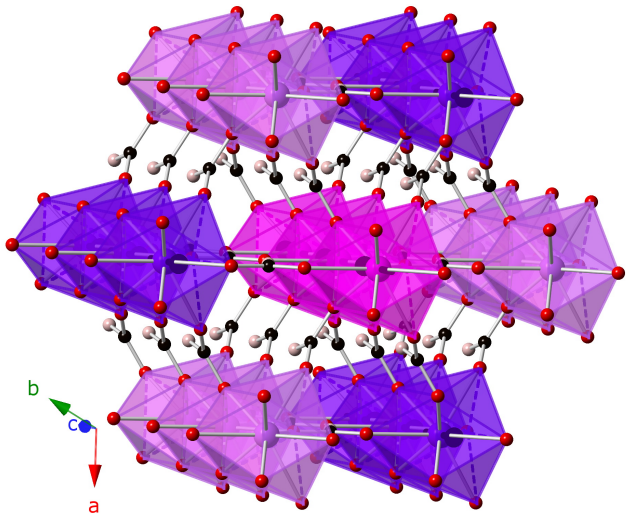

Fig. 17: Structure of $Tb(Fm)_3$ highlighting the face-sharing chains in this structure and showing its PDA average magnetic structure.[112] The polyhedral with distinct colours are the three spin states in this model and all other colours are the same as in Fig. 1.

More extensive RMC studies using the unique high resolution capabilities of the WISH neutron diffractometer,[114] showed that the Ising-like anisotropy and intrachain ferromagnetic correlations become significant below 10 K.[111] Monte Carlo models were able to reproduce the temperature evolution of the magnetic correlations observed from RMC fits to $Tb(Fm)_3$ when the Ising like anisotropy was set to 70(20) K, J_{intra} = -1.5(5) K and J_{inter} = 0.03(1) K; confirming the strong Ising-like nature of the system and its strongly low-dimensional nature.[111] More intriguingly this Monte Carlo model suggested the emergence of a state below 1.6 K, which had long-range ordered ferromagnetic chains but, because of antiferromagnetic frustration on the triangular lattice, no 3D magnetic order. Viewing each chain as having a single

collective spin this state is a realization of the Triangular Ising Antiferromagnet (TIA); RMC fits of such a TIA model to the combination of sharp and diffuse magnetic scattering observed at 1.6 K successfully reproduce these features while conventional crystallographic models, such as the PDA, are unable to fit the diffuse magnetic scattering (see Fig. 18).[111] While the sharp magnetic reflections are broader than expected for Bragg peaks this is only revealed by the uniquely high resolution of the WISH instrument; conventional analysis using data collected on neutron diffractometers routinely used for the magnetic structure determinations discussed in this review would show no indication of this state not being 3D ordered if, as is commonly the case including previous studies of $Tb(Fm)_3$, the structured diffuse scattering is overlooked. The coincident combination of sharp and diffuse scattering is, however, of precisely the form theoretically expected for a TIA state,[115] highlighting the need to take care with interpreting magnetic scattering from both MOFs and conventional magnetic materials featuring indications of frustration and/or low dimensionality.

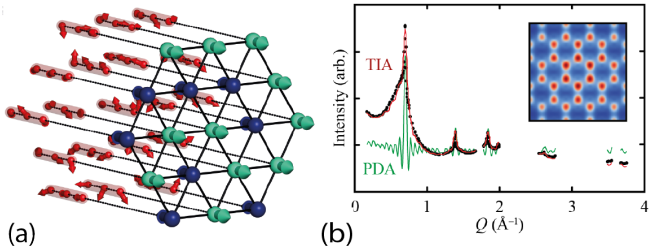

Fig. 18: a) The TIA phase that emerges from a joint refinement of the Bragg-like and diffuse magnetic scattering observed in the diffraction pattern shown in b).[111] Average structure models such as the PDA model cannot fit the diffuse magnetic scattering observed as indicated by the fit shown in b). Bragg-like features appear at the regions of reciprocal space associated with maxima in the TIA diffuse scattering pattern (insert).

Summary and Perspective

This review has highlighted the great insight that can be obtained from magnetic MOFs and coordination polymers by probing their interactions at the atomic scale, chiefly using neutron scattering and DFT. As shown by the compounds reviewed above such approaches allow the different interactions in these complex magnetic materials to be resolved, including their magnetic dimensionality and, thereby correct misinterpretations that often arise from analyzing physical property measurements through geometric considerations alone. Additionally microscopic analysis of MOFs can provide insight into the differences between the myriad of magnetic phases that can arise in these materials with changing magnetic cation, temperature, magnetic field or pore content. Such studies can also identify unique magnetic phenomena in MOFs, including spin-idle,[99] long range 1D magnetic order[111] and closing of the Haldane gap[87, 89].

The good news is rapid advances in techniques are beginning to make a wider range of MOFs and coordination frameworks amenable to such studies, as highlighted by the case studies presented above. Modern instruments with greater neutron flux have enabled neutron diffraction to be applied to non-deuterated powder samples of only a few hundred mgs. Around 40 % of the families mentioned in this review have significant hydrogen content, up to about 50 atom %, but have still had their magnetic structures solved by powder neutron diffraction without deuteration. Deuterated powder samples will always provide much higher quality data, required to resolve the full details of more complex magnetic materials. The ability, however, to study a wider range of hydrogenated samples in the future opens up neutron scattering to compounds that cannot be feasibly deuterated or where initial data is needed to justify the significant time and expense invested in perdeuteration. Almost all of these high-hydrogen content samples have had their magnetic structures analysed using high flux instruments at reactor sources, avoiding concerns with multi-wavelength dependant attenuation corrections at time-of-flight based instruments.[38, 40, 57, 75, 84, 116] This emphasises the importance of both continued access to reactor-based neutrons and more robust data correction from modern spallation sources.

Highly intense neutron sources, particularly modern spallation sources, also have an important role to play in opening up more MOFs to single crystal magnetic diffraction studies. Such single crystal studies potentially enable samples with more complex structures and higher hydrogen content to be studied, since the background caused by the incoherent scattering of hydrogen is less problematic in single crystal measurements, than can be done with neutron powder diffraction. This would build on the scarce examples discussed in this review, which, with one exception,[40] all required single crystals in excess of 10 mm^3,[68, 88, 89] rarely available for most MOFs. Laue neutron diffractometers,[117, 118] have already been used to study 1 mm^3 sized samples of magnetic oxides and new instruments at the SNS, the JPARC MLF and forthcoming ESS in principal push these limits further,[119] as likely required for more magnetically dilute MOFs.

As highlighted by this review the use of inelastic scattering to study the dynamics of magnetic MOFs is also a growing area, although reported inelastic neutron scattering studies on MOFs still require deuterated samples on the gram scale. Recent studies have indicated that measurements are possible on hydrogenous samples using the high intensities of modern time-of-flight spectrometers[75, 120] and such measurements are likely to grow with source intensities and increasing availability of neutron polarisation capabilities that enables magnetic scattering to be subtracted from other contributions to neutron scattering patterns. Continued software developments that enable a wider range of non-expert users to take advantage of neutron scattering, through for example the ability to rapidly determine magnetic structures through representation and distortion mode analysis,[52, 121] or applying RMC methods to local structure refinements, will also play a key role in the further development of this field.

While providing significant understanding to complement experimental studies, currently first principles calculations of magnetic frameworks appear to be limited to mainly support

experimental studies for some of the less complex magnetic systems. For predictive investigations, future methods will likely require a higher-level theory to negate the use of fitting parameters. The study of (partially) disordered, frustrated, or dynamical magnetic systems may make more use of "effective Hamiltonians", whereby the fully non-colinear spin interactions are extracted from first principles, allowing for computationally tractable dynamical studies. Nevertheless, due to inherent approximations or coarse graining required to make calculations feasible, we suggest the collaborative effort between first principles and neutron studies will likely be key to shed light on magnetic frameworks in the foreseeable future.

Conflicts of interest

There are no conflicts to declare.

References

1. a) W. Eerenstein, N. D. Mathur and J. F. Scott, *Nature*, 2006, **442**, 759-765; b) J. F. Scott, *Nat. Mater.*, 2007, **6**, 256-257; c) N. Ortega, K. Ashok, J. F. Scott and S. K. Ram, *J. Phys. Condens. Mat.*, 2015, **27**, 504002;.
2. a) P. Dechambenoit and J. R. Long, *Chem. Soc. Rev.*, 2011, **40**, 3249-3265; b) E. Coronado, M. Giménez-Marqués, G. M. Espallargas and L. Brammer, *Nat. Commun.*, 2012, **3**, 828.
3. a) J. Mohd Jani, M. Leary, A. Subic and M. A. Gibson, *Mater. Design*, 2014, **56**, 1078-1113; b) D. Makarov, M. Melzer, D. Karnaushenko and O. G. Schmidt, *Appl. Phys. Rev.*, 2016, **3**, 011101.
4. Y.-Z. Zheng, G.-J. Zhou, Z. Zheng and R. E. P. Winpenny, *Chem. Soc. Rev.*, 2014, **43**, 1462-1475.
5. G. Lorusso, J. W. Sharples, E. Palacios, O. Roubeau, E. K. Brechin, R. Sessoli, A. Rossin, F. Tuna, E. J. L. McInnes, D. Collison and M. Evangelisti, *Adv. Mater.*, 2013, **25**, 4653-4656.
6. a) A. P. Ramirez, *Annu. Rev. Mater. Sci.*, 1994, **24**, 453-480; b) R. Moessner and A. P. Ramirez, *Phys. Today*, 2006, **59**, 24-29; c) J. T. Chalker, in *Introduction to Frustrated Magnetism: Materials, Experiments, Theory*, eds. C. Lacroix, P. Mendels and F. Mila, Springer Berlin Heidelberg, Berlin, Heidelberg, 2011, pp. 3-22.
7. a) H. J. Mikeska and M. Steiner, *Adv. Phys.*, 1991, **40**, 191-356; b) S. Sahling, G. Remenyi, C. Paulsen, P. Monceau, V. Saligrama, C. Marin, A. Revcolevschi, L. P. Regnault, S. Raymond and J. E. Lorenzo, *Nat. Phys.*, 2015, **11**, 255-260.
8. V. Garcia, M. Bibes, L. Bocher, S. Valencia, F. Kronast, A. Crassous, X. Moya, S. Enouz-Vedrenne, A. Gloter, D. Imhoff, C. Deranlot, N. D. Mathur, S. Fusil, K. Bouzehouane and A. Barthélémy, *Science*, 2010, **327**, 1106-1110.
9. a) G. J. Halder, C. J. Kepert, B. Moubaraki, K. S. Murray and J. D. Cashion, *Science*, 2002, **298**, 1762-1765; b) Z. Wang, B. Zhang, H. Fujiwara, H. Kobayashi and M. Kurmoo, *Chem. Commun.*, 2004, 416-417.
10. C. Train, M. Gruselle and M. Verdaguer, *Chem. Soc. Rev.*, 2011, **40**, 3297-3312.
11. a) G. Rogez, N. Viart and M. Drillon, *Angew. Chem. Int. Ed.*, 2010, **49**, 1921-1923; b) Z. Wang, K. Hu, S. Gao and H. Kobayashi, *Adv. Mater.*, 2010, **22**, 1526-1533.
12. D. Tiana, C. H. Hendon and A. Walsh, *Chem. Commun.*, 2014, **50**, 13990-13993.
13. a) S. R. Batten, N. R. Champness, X.-M. Chen, J. Garcia-Martinez, S. Kitagawa, L. Ohrstrom, M. O'Keeffe, M. P. Suh and J. Reedijk, *CrystEngComm*, 2012, **14**, 3001-3004; b) S. Seth and A. J. Matzger, *Cryst. Growth Des.*, 2017, **17**, 4043-4048.
14. a) M. Kurmoo, *Chem. Soc. Rev.*, 2009, **38**, 1353 -1379; b) G. E. Kostakis, I. J. Hewitt, A. M. Ako, V. Mereacre and A. K. Powell, *Philos. T. R. Soc. A*, 2010, **368**, 1509; c) E. Coronado and G. Minguez Espallargas, *Chem. Soc. Rev.*, 2013, **42**, 1525-1539.
15. B. T. M. Willis and C. J. Carlile, *Experimental Neutron Scattering*, Oxford University Press, Oxford, United Kingdom, 2013.
16. L. E. Smart and E. A. Moore, *Solid State Chemistry: An Introduction*, CRC Press, Boca Raton, Florida, Fourth edn., 2012.
17. a) C. Vettier, *Eur. Phys. J. Spec. To.*, 2012, **208**, 3-14; b) P. G. Radaelli and S. S. Dhesi, *Philos. T. R. Soc. A*, 2015, **373**, 20130148.
18. a) T. Gibb, *Principles of Mössbauer Spectroscopy*, Spinger Dordrecht, 1976; b) A. Schenck, *Muon Spin Rotation Spectroscopy: Principles and Applications in Solid State Physics*, Adam Hilger, Bristol, 1985.
19. C. G. Shull, W. A. Strauser and E. O. Wollan, *Phys. Rev.*, 1951, **83**, 333-345.
20. P. Day, *Inorg. Chim. Acta*, 2008, **361**, 3365-3370.
21. M. T. Weller, P. F. Henry, V. P. Ting and C. C. Wilson, *Chem. Commun.*, 2009, 2973-2989.
22. P. Hohenberg and W. Kohn, *Phys. Rev.*, 1964, **136**, B864-B871.
23. W. Kohn and L. J. Sham, *Phys. Rev.*, 1965, **140**, A1133-A1138.
24. U. v. Barth and L. Hedin, *J. Phys. C*, 1972, **5**, 1629-1642.
25. S. Grimme, *Wires. Comput. Mol. Sci.*, 2011, **1**, 211-228.
26. V. I. Anisimov, J. Zaanen and O. K. Andersen, *Phys. Rev. B*, 1991, **44**, 943-954.
27. a) M. Cococcioni and S. de Gironcoli, *Phys. Rev. B*, 2005, **71**, 035105; b) H. J. Kulik, M. Cococcioni, D. A. Scherlis and N. Marzari, *Phys. Rev. Lett.*, 2006, **97**, 103001.
28. P. Burlet, P. Burlet, J. Rossat-Mignod, A. De combarieu and E. Bedin, *Phys. Status Solidi B*, 1975, **71**, 675-685.
29. D. G. Kellerman, Y. A. Barykina, K. A. Zheleznikov, A. P. Tyutyunnik and V. N. Krasilnikov, *Phys. Status Solidi B*, 2016, **253**, 2209-2216.
30. M. R. V. Jørgensen, M. Christensen, M. S. Schmøkel and B. B. Iversen, *Inorg. Chem.*, 2011, **50**, 1441-1446.
31. R. Kiriyama, H. Ibamoto and K. Matsuo, *Acta Crystallogr.*, 1954, **7**, 482-483.
32. N. Burger, H. Fuess and P. Burlet, *Solid State Commun.*, 1980, **34**, 883-886.
33. K. Koyama, H. Nobumasa and M. Matsuura, *J. Phys. Soc. Jpn.*, 1987, **56**, 1553-1561.
34. S. J. Clarke, A. Harrison, T. E. Mason, G. J. McIntyre and D. Visser, *J. Phys. Condens. Mat.*, 1992, **4**, L71-L76.
35. S. J. Clarke, A. Harrison, T. E. Mason and D. Visser, *Solid State Commun.*, 1999, **112**, 561-564.
36. H. M. Rønnow, D. F. McMorrow and A. Harrison, *Phys. Rev. Lett.*, 1999, **82**, 3152-3155.
37. M.-H. Zeng, M.-C. Wu, H. Liang, Y.-L. Zhou, X.-M. Chen and S.-W. Ng, *Inorg. Chem.*, 2007, **46**, 7241-7243.
38. O. Fabelo, L. Cañadillas-Delgado, I. Puente Orench, J. A. Rodríguez-Velamazán, J. Campo and J. Rodríguez-Carvajal, *Inorg. Chem.*, 2011, **50**, 7129-7135.

39. K. S. Hagen, S. G. Naik, B. H. Huynh, A. Masello and G. Christou, *J. Am. Chem. Soc.*, 2009, **131**, 7516-7517.
40. L. Cañadillas-Delgado, O. Fabelo, J. A. Rodríguez-Velamazán, M.-H. Lemée-Cailleau, S. A. Mason, E. Pardo, F. Lloret, J.-P. Zhao, X.-H. Bu, V. Simonet, C. V. Colin and J. Rodríguez-Carvajal, *J. Am. Chem. Soc.*, 2012, **134**, 19772-19781.
41. A. S. Wills, *J. Mater. Chem.*, 2005, **15**, 245-252.
42. J.-P. Zhao, B.-W. Hu, F. Lloret, J. Tao, Q. Yang, X.-F. Zhang and X.-H. Bu, *Inorg. Chem.*, 2010, **49**, 10390-10399.
43. L. Mazzuca, L. Cañadillas-Delgado, J. A. Rodríguez-Velamazán, O. Fabelo, M. Scarrozza, A. Stroppa, S. Picozzi, J.-P. Zhao, X.-H. Bu and J. Rodríguez-Carvajal, *Inorg. Chem.*, 2017, **56**, 197-207.
44. E. M. Bauer, C. Bellitto, M. Colapietro, G. Portalone and G. Righini, *Inorg. Chem.*, 2003, **42**, 6345-6351.
45. G. Nénert, U. Adem, E. M. Bauer, C. Bellitto, G. Righini and T. T. M. Palstra, *Phys. Rev. B*, 2008, **78**, 054443.
46. G. Nénert, H.-J. Koo, C. V. Colin, E. M. Bauer, C. Bellitto, C. Ritter, G. Righini and M.-H. Whangbo, *Inorg. Chem.*, 2013, **52**, 753-760.
47. P. Jain, V. Ramachandran, R. J. Clark, H. D. Zhou, B. H. Toby, N. S. Dalal, H. W. Kroto and A. K. Cheetham, *J. Am. Chem. Soc.*, 2009, **131**, 13625-13627.
48. a) H. D. Duncan, M. T. Dove, D. A. Keen and A. E. Phillips, *Dalton Trans.*, 2016, **45**, 4380-4391; b) L. Mazzuca, L. Cañadillas-Delgado, O. Fabelo, J. A. Rodríguez-Velamazán, J. Luzón, O. Vallcorba, V. Simonet, C. V. Colin and J. Rodríguez-Carvajal, *Chem. Eur. J.*, 2018, **24**, 388-399.
49. J. M. M. Lawler, P. Manuel, A. L. Thompson and P. J. Saines, *Dalton Trans.*, 2015, **44**, 11613-11620.
50. Z. Wang, B. Zhang, K. Inoue, H. Fujiwara, T. Otsuka, H. Kobayashi and M. Kurmoo, *Inorg. Chem.*, 2007, **46**, 437-445.
51. G.-C. Xu, W. Zhang, X.-M. Ma, Y.-H. Chen, L. Zhang, H.-L. Cai, Z.-M. Wang, R.-G. Xiong and S. Gao, *J. Am. Chem. Soc.*, 2011, **133**, 14948-14951.
52. B. J. Campbell, H. T. Stokes, D. E. Tanner and D. M. Hatch, *J. Appl. Crystallogr.*, 2006, **39**, 607-614.
53. Y. Sun, Z. Zhuo and X. Wu, *RSC Adv.*, 2016, **6**, 113234-113239.
54. S. Kibayashi, Y. Takahashi, S. Seki and Y. Tokura, *Nat. Commun.*, 2014, **5**, 4583.
55. a) N. S. Kiselev, A. N. Bogdanov, R. Schäfer and U. K. Rößler, *J. Phys. D*, 2011, **44**, 392001; b) N. Nagaosa and Y. Tokura, *Nat. Nano.*, 2013, **8**, 899-911.
56. A. Hoshikawa, T. Kamiyama, A. Purwanto, K. Ohishi, W. Higemoto, T. Ishigaki, H. Imai and K. Inoue, *J. Phys. Soc. Jpn.*, 2004, **73**, 2597-2600.
57. R. Feyerherm, A. Loose, T. Ishida, T. Nogami, J. Kreitlow, D. Baabe, F. J. Litterst, S. Süllow, H. H. Klauss and K. Doll, *Phys. Rev. B*, 2004, **69**, 134427.
58. R. Andrés, M. Brissard, M. Gruselle, C. Train, J. Vaissermann, B. Malézieux, J.-P. Jamet and M. Verdaguer, *Inorg. Chem.*, 2001, **40**, 4633-4640.
59. P. Fabrice, G. Michel, A. Gilles and T. Cyrille, *J. Phys. Condens. Mat.*, 2008, **20**, 135214.
60. S. Mühlbauer, B. Binz, F. Jonietz, C. Pfleiderer, A. Rosch, A. Neubauer, R. Georgii and P. Böni, *Science*, 2009, **323**, 915-919.
61. H. N. Bordallo, L. Chapon, J. L. Manson, J. Hernández-Velasco, D. Ravot, W. M. Reiff and D. N. Argyriou, *Phys. Rev. B*, 2004, **69**, 224405.
62. D. Ghoshal, T. Kumar Maji, T. Mallah, T.-H. Lu, G. Mostafa and N. R. Chaudhuri, *Inorg. Chim. Acta*, 2005, **358**, 1027-1033.
63. G. Rousse, G. Radtke, Y. Klein and H. Ahouari, *Dalton Trans.*, 2016, **45**, 2536-2548.
64. Z.-L. Huang, M. Drillon, N. Masciocchi, A. Sironi, J.-T. Zhao, P. Rabu and P. Panissod, *Chem. Mater.*, 2000, **12**, 2805-2812.
65. R. Sibille, A. Mesbah, T. Mazet, B. Malaman, S. Capelli and M. François, *J. Solid State Chem.*, 2012, **186**, 134-141.
66. A. Mesbah, R. Sibille, T. Mazet, B. Malaman, S. Lebegue and M. Francois, *J. Mater. Chem.*, 2010, **20**, 9386-9391.
67. R. Feyerherm, A. Loose, P. Rabu and M. Drillon, *Solid State Sci.*, 2003, **5**, 321-326.
68. P. Díaz-Gallifa, O. Fabelo, J. Pasán, L. Cañadillas-Delgado, J. Rodríguez-Carvajal, F. Lloret, M. Julve and C. Ruiz-Pérez, *Inorg. Chem.*, 2014, **53**, 5674-5683.
69. P. J. Saines, B. C. Melot, R. Seshadri and A. K. Cheetham, *Chem. Eur. J.*, 2010, **16**, 7579-7585.
70. P. J. Saines, J. R. Hester and A. K. Cheetham, *Phys. Rev. B*, 2010, **82**, 144435.
71. S. Kanungo and T. Saha-Dasgupta, *Phys. Rev. B*, 2011, **84**, 134415.
72. P. J. Saines, P. T. Barton, M. Jura, K. S. Knight and A. K. Cheetham, *Mater. Horiz.*, 2014, **1**, 332-337.
73. P. J. Saines, P. T. Barton, P. Jain and A. K. Cheetham, *CrystEngComm*, 2012, **14**, 2711-2720.
74. K. L. Svane, P. J. Saines and A. Walsh, *J. Mater. Chem. C*, 2015, **3**, 11076-11080.
75. J. L. Manson, Q.-z. Huang, C. M. Brown, J. W. Lynn, M. B. Stone, J. Singleton and F. Xiao, *Inorg. Chem.*, 2015, **54**, 11897-11905.
76. J. L. Manson, C. D. Incarvito, A. L. Rheingold and J. S. Miller, *J. Chem. Soc. Dalton Trans.*, 1998, 3705-3706.
77. a) P. Jensen, S. R. Batten, G. D. Fallon, D. C. R. Hockless, B. Moubaraki, K. S. Murray and R. Robson, *J. Solid State Chem.*, 1999, **145**, 387-393; b) P. Jensen, S. R. Batten, B. Moubaraki and K. S. Murray, *J. Solid State Chem.*, 2001, **159**, 352-361.
78. J. Manson, T. Lancaster, S. J. Blundell, Y. Qiu, J. Singleton, P. Sengupta, F. L. Pratt, J. Kang, C. Lee and M.-H. Whangbo, *Polyhedron*, 2010, **29**, 514-520.
79. J. L. Manson, Q.-z. Huang, J. W. Lynn, H.-J. Koo, M.-H. Whangbo, R. Bateman, T. Otsuka, N. Wada, D. N. Argyriou and J. S. Miller, *J. Am. Chem. Soc.*, 2001, **123**, 162-172.
80. J. L. Manson, L. C. Chapon, H. N. Bordallo, R. Feyerherm, D. N. Argyriou and A. Loose, *J. Magn. Magn. Mater.*, 2003, **260**, 462-466.
81. J. L. Manson, H. N. Bordallo, J. W. Lynn, Q. Huang, R. Feyerherm, A. Loose, L. Chapon and D. N. Argyriou, *Appl. Phys. A*, 2002, **74**, s722-s724.
82. S. Blundell, *Magnetism in Condensed Matter*, Oxford University Press, Oxford, UK, 2014.
83. R. Sibille, T. Mazet, B. Malaman, T. Gaudisson and M. François, *Inorg. Chem.*, 2012, **51**, 2885-2892.
84. R. Sibille, E. Lhotel, T. Mazet, B. Malaman, C. Ritter, V. Ban and M. François, *Phys. Rev. B*, 2014, **89**, 104413.
85. I. Affleck, *Phys. Rev. B*, 1991, **43**, 3215-3222.
86. M. Monfort, J. Ribas, X. Solans and M. Font-Bardía, *Inorg. Chem.*, 1996, **35**, 7633-7638.
87. Z. Honda, K. Katsumata, H. A. Katori, K. Yamada, T. Ohishi, T. Manabe and M. Yamashita, *J. Phys. Condens. Mat.*, 1997, **9**, L83-L88.
88. A. Zheludev, Z. Honda, K. Katsumata, R. Feyerherm and K. Prokes, *EPL Europhys. Lett.*, 2001, **55**, 868-873.
89. Y. Chen, Z. Honda, A. Zheludev, C. Broholm, K. Katsumata and S. M. Shapiro, *Phys. Rev. Lett.*, 2001, **86**, 1618-1621.
90. A. Zheludev, Z. Honda, Y. Chen, C. L. Broholm, K. Katsumata and S. M. Shapiro, *Phys. Rev. Lett.*, 2002, **88**, 077206.

91. A. Zheludev, B. Grenier, E. Ressouche, L. P. Regnault, Z. Honda and K. Katsumata, *Phys. Rev. B*, 2005, **71**, 104418.
92. D. S. Yufit, J. A. K. Howard, D. J. Price, S. O. H. Gutschke, A. K. Powell and P. T. Wood, *Chem. Commun.*, 1999, 1561-1562.
93. R. A. Mole, J. A. Stride, A. S. Wills and P. T. Wood, *Physica B*, 2006, **385**, 435-437.
94. R. A. Mole, S. P. Cottrell, J. A. Stride and P. T. Wood, *Inorg. Chimica Acta*, 2008, **361**, 3718-3722.
95. R. A. Mole, J. A. Stride, T. Unruh and P. T. Wood, *J. Phys. Condens. Mat.*, 2009, **21**, 076003.
96. C. Castelnovo, R. Moessner and S. L. Sondhi, *Nature*, 2008, **451**, 42-45.
97. H. Nakamura, K. Yoshimoto, M. Shiga, M. Nishi and K. Kakurai, *J. Phys. Conden. Mat.*, 1997, **9**, 4701.
98. M. Kurmoo, H. Kumagai, K. W. Chapman and C. J. Kepert, *Chem. Commun.*, 2005, 3012-3014.
99. R. A. Mole, J. A. Stride, P. F. Henry, M. Hoelzel, A. Senyshyn, A. Alberola, C. J. Gómez Garcia, P. R. Raithby and P. T. Wood, *Inorg. Chem.*, 2011, **50**, 2246-2251.
100. S. O. H. Gutschke, M. Molinier, A. K. Powell and P. T. Wood, *Angew. Chem. Int. Ed.*, 1997, **36**, 991-992.
101. R. A. Mole, M. A. Nadeem, J. A. Stride, V. K. Peterson and P. T. Wood, *Inorg. Chem.*, 2013, **52**, 13462-13468.
102. A. M. Richard, C. R. Kirrily, Y. Dehong, A. S. John, M. A. Nadeem and T. W. Paul, *J. Phys. Conden. Mat.*, 2016, **28**, 126005.
103. a) J. L. Manson, C. Campana and J. S. Miller, *Chem. Commun.*, 1998, 251-252; b) H. Hoshino, K. Iida, T. Kawamoto and T. Mori, *Inorg. Chem.*, 1999, **38**, 4229-4232; c) M. Kurmoo, *Mol. Cryst. Liq. Cryst. A*, 2000, **342**, 167-176.
104. R. Feyerherm, A. Loose and J. L. Manson, *J. Phys. Condens. Mat.*, 2003, **15**, 663-673.
105. R. Feyerherm, A. Loose, S. Landsgesell and J. L. Manson, *Inorg. Chem.*, 2004, **43**, 6633-6639.
106. J. L. Manson, E. Ressouche and J. S. Miller, *Inorg. Chem.*, 2000, **39**, 1135-1141.
107. C. R. Kmety, J. L. Manson, Q. Huang, J. W. Lynn, R. W. Erwin, J. S. Miller and A. J. Epstein, *Phys. Rev. B*, 1999, **60**, 60-63.
108. C. R. Kmety, Q. Huang, J. W. Lynn, R. W. Erwin, J. L. Manson, S. McCall, J. E. Crow, K. L. Stevenson, J. S. Miller and A. J. Epstein, *Phys. Rev. B*, 2000, **62**, 5576-5588.
109. D. O. Demchenko, A. Y. Liu, E. Z. Kurmaev, L. D. Finkelstein, V. R. Galakhov, A. Moewes, S. G. Chiuzbăian, M. Neumann, C. R. Kmety and K. L. Stevenson, *Phys. Rev. B*, 2004, **69**, 205105.
110. a) J. A. M. Paddison and A. L. Goodwin, *Phys. Rev. Lett.*, 2012, **108**, 017204; b) J. A. M. Paddison, J. R. Stewart and A. L. Goodwin, *J. Phys. Condens. Mat.*, 2013, **25**, 454220.
111. D. R. Harcombe, P. G. Welch, P. Manuel, P. J. Saines and A. L. Goodwin, *Phys. Rev. B*, 2016, **94**, 174429.
112. P. J. Saines, J. A. M. Paddison, P. M. M. Thygesen and M. G. Tucker, *Mater. Horiz.*, 2015, **2**, 528-535.
113. A. I. Kurbakov, J. Rodriguez-Carvajal, V. Trounov and N. V. Starostina, *Mater. Sci. Forum*, 2000, **321-324**, 971-975.
114. L. C. Chapon, P. Manuel, P. G. Radaelli, C. Benson, L. Perrott, S. Ansell, N. J. Rhodes, D. Raspino, D. Duxbury, E. Spill and J. Norris, *Neutron News*, 2011, **22**, 22-25.
115. a) D. H. Wojtas and R. P. Millane, *Phys. Rev. E*, 2009, **79**, 041123; b) C. Yoon and R. P. Millane, *J. Opt. Soc. Am. A*, 2014, **31**, 1416-1426.
116. A. Mesbah, B. Malaman, T. Mazet, R. Sibille and M. Francois, *CrystEngComm*, 2010, **12**, 3126-3131.
117. A. J. Edwards, *Aust. J. Chem.*, 2011, **64**, 869-872.
118. B. Ouladdiaf, J. Archer, J. R. Allibon, P. Decarpentrie, M.-H. Lemee-Cailleau, J. Rodriguez-Carvajal, A. W. Hewat, S. York, D. Brau and G. J. McIntyre, *J. Appl. Crystallogr.*, 2011, **44**, 392-397.
119. T. Ohhara, R. Kiyanagi, K. Oikawa, K. Kaneko, T. Kawasaki, I. Tamura, A. Nakao, T. Hanashima, K. Munakata, T. Moyoshi, T. Kuroda, H. Kimura, T. Sakakura, C.-H. Lee, M. Takahashi, K.-i. Ohshima, T. Kiyotani, Y. Noda and M. Arai, *J. Appl. Crystallogr.*, 2016, **49**, 120-127.
120. R. A. Mole, S. Greene, P. F. Henry, S. M. Humphrey, K. C. Rule, T. Unruh, G. F. Weldon, D. Yu, J. A. Stride and P. T. Wood, *Inorg. Chem.*, 2017, **56**, 7851-7860.
121. A. S. Wills, *Acta Crystallogr. A*, 2008, **A64**, C107.

1